NASA TECHNICAL MEMORANDUM

NASA TM X-3215

NASA TM X-3215

TRANSONIC OFF-DESIGN DRAG AND PERFORMANCE OF THREE MIXED-COMPRESSION AXISYMMETRIC INLETS

Richard R. Woollett, Edward T. Melcason, and David A. Choby

Lewis Research Center
Cleveland, Ohio 44135

NATIONAL AERONAUTICS AND SPACE ADMINISTRATION • WASHINGTON, D. C. • JUNE 1975

1. Report No.	2. Government Accession No.	3. Recipient's Catalog No.
NASA TM X-3215		

4. Title and Subtitle	5. Report Date
TRANSONIC OFF-DESIGN DRAG AND PERFORMANCE OF THREE MIXED-COMPRESSION AXISYMMETRIC INLETS	June 1975
	6. Performing Organization Code

7. Author(s)	8. Performing Organization Report No.
Richard R. Woollett, Edward T. Meleason, and David A. Choby	E-8146
	10. Work Unit No. 505-04

9. Performing Organization Name and Address	11. Contract or Grant No.
Lewis Research Center National Aeronautics and Space Administration Cleveland, Ohio 44135	
	13. Type of Report and Period Covered
12. Sponsoring Agency Name and Address	Technical Memorandum
National Aeronautics and Space Administration Washington, D.C. 20546	14. Sponsoring Agency Code

15. Supplementary Notes

16. Abstract

An experimental investigation was conducted to determine the off-design drag and pressure performance of three axisymmetric supersonic inlets in the transonic speed range. For typical engine airflows at Mach 0.8 the drag coefficient varied from 0.045 to 0.09; at Mach 1.2 the largest drag coefficient measured was 0.25. Below Mach 0.9 a lower drag resulted when all or at least part of the excess weight flow was spilled over the cowl rather than through the bypass doors; above Mach 1.1 the lowest drag was obtained by bypassing excess flow.

17. Key Words (Suggested by Author(s))	18. Distribution Statement
Transonic drag Inlets Additive drag Spillage drag	Unclassified - unlimited STAR category 07 (rev.)

19. Security Classif. (of this report)	20. Security Classif. (of this page)	21. No. of Pages	22. Price*
Unclassified	Unclassified	49	$3.75

* For sale by the National Technical Information Service, Springfield, Virginia 22151

TRANSONIC OFF-DESIGN DRAG AND PERFORMANCE OF THREE MIXED-COMPRESSION AXISYMMETRIC INLETS

by Richard R. Woollett, Edward T. Meleason, and David A. Choby

Lewis Research Center

SUMMARY

An experimental investigation was conducted to determine the off-design drag and pressure performance of three axisymmetric supersonic inlets in the transonic speed range. The inlets listed in order of increasing drag at Mach 0.8 were 30-70, 60-40, and 40-60, where the numbers indicate the percentage of external and internal contraction, respectively, that existed at the design speeds of Mach 2.7, 2.5, and 2.5, respectively. At Mach 0.8 with typical engine airflows the drag coefficient varied from 0.045 to 0.09. At Mach 1.2 the largest drag coefficient measured was 0.25 with the 60-40 inlet. In general, the drag characteristics of these inlets (including additive and cowl pressure drag) exhibited the typical drag rise near Mach 1. Below Mach 0.9 a lower drag resulted when all or at least part of the excess weight flow was spilled over the cowl rather than through the bypass doors. Above Mach 1.1 the lowest drag of the 60-40 and 40-60 inlets was obtained by bypassing excess flow.

INTRODUCTION

When supersonic inlets are flown at transonic speeds, the engine may require only about 60 percent of the capture mass flow. The manner in which the excess mass flow is spilled affects the drag of the nacelle. It has been estimated that the drag penalty associated with spilling this air on a Mach 2.7 transport can be as much as 3 percent of the payload, even though the air is spilled only during acceleration and deceleration of the vehicle through the sonic region (ref. 1). If a flight pattern over land at high subsonic speeds or even a holding pattern is required, the fuel consumption will depend directly upon the subsonic drag and consequently on how the excess air is dumped overboard. The required fuel reserve for a possible holding pattern and for use during acceleration can easily be equal to the weight of the payload (ref. 2). Therefore, any reduction in subsonic and transonic drag can significantly affect the payload.

The NASA Lewis Research Center is conducting tests to evaluate the performance characteristics of a series of supersonic inlets at off-design conditions. This report presents data for three axisymmetric inlets that were tested under this program. The design Mach number of the series of inlets varies from 2.5 to 2.7. The design configurations of two mixed-compression inlets, a 60-40 inlet and a 40-60 inlet (where the numbers indicate the percentage of external and internal contraction, respectively), were tested at a Mach number of 2.5 (refs. 3 and 4, respectively). The configuration of a third mixed-compression inlet, a 30-70 inlet, was designed for Mach 2.7 and was similar to the N_5 inlet reported in reference 5. The transonic and subsonic configurations of the three inlets were formed by collapsing or translating various centerbody and internal cowl surfaces or both. Another version of the 60-40 inlet was tested, and the results are reported in reference 6. This modification of the 60-40 inlet was achieved by translating the collapsed centerbody of the inlet forward to eliminate internal contraction that existed when the centerbody was collapsed in place. The modifications for each of the inlets would provide adequate weight flow for a typical turbojet engine during transonic operation.

There are three ways in which air can be spilled at transonic speeds with fixed cowl inlets: (1) flow deflection ahead of the cowl by means of the centerbody, (2) spillage over the cowl caused by not accepting the flow internally, and (3) taking the flow on board and then dumping it through bypass doors ahead of the compressor face. Deflection of the flow by a centerbody ahead of the cowl lip is normally best but is limited by geometry. The flight condition where it is best to bypass the additional flow rather than spilling it ahead of the cowl lip varies with the individual inlet.

The transonic performance, including compressor face total-pressure recovery, steady-state distortion, dynamic distortion, and cowl and centerbody surface static pressures, is presented. Total inlet drag is also presented, as well as its various components of additive, cowl, and friction drags.

The transonic tests were conducted in the Lewis Research Center 8- by 6-Foot Supersonic Wind Tunnel over a Mach range of 0.8 to 1.27. For the 25.4-centimeter-diameter models tested the inlet Reynolds number was nominally 3.7×10^6. Although U.S. customary units were specified when the model was fabricated, all the dimensions given in this report are in SI units. All the symbols are defined in appendix A.

APPARATUS AND PROCEDURE

Models

The inlet contours of the transonic 60-40 inlet were obtained by modifying the centerbody coordinates of a double-cone inlet tested earlier at Mach 2.5 (ref. 3). The area

contraction of a capture stream tube from the free stream to the throat of the inlet at the design Mach number of 2.5 was approximately 60 percent external and 40 percent internal. The transonic centerbody surface simulates a configuration where the second cone of the design inlet was collapsed to the first cone angle. This change results in an entrance to throat area ratio of 1.118. The inlet tested in the study of reference 6 removed this residual internal contraction by translation of the centerbody. The surface coordinates of the 60-40 inlet and the area variations of both the design and transonic versions of the inlet are plotted in figure 1(a). Table I(a) lists the nondimensional coordinates of the off-design inlet from the tip of the centerbody downstream to the compressor face. The capture area A_c and cowl entrance diameter D_c of the 60-40 inlet are 375.8 square centimeters and 21.87 centimeters, respectively.

The inlet contours of the transonic 40-60 inlet were obtained by modifying the centerbody coordinates of a single-cone (12.5° half-angle) inlet tested earlier at Mach 2.5 (ref. 4). At the design Mach number of 2.5 the area contraction of a capture stream tube of the design inlet was 40 percent external and 60 percent internal. The transonic centerbody surface simulates a configuration where the centerbody surfaces of the design inlet were collapsed about four hinge points, the first of which was in the plane of the cowl lip and the last of which was at the compressor face (fig. 1(b)). The coordinates of the external compression surface remain unchanged. These changes of the 40-60 inlet result in an entrance to throat area ratio of 1.04. The surface coordinates and the area variations of both the design and transonic versions of the 40-60 inlet are plotted in figure 1(b). Table I(b) lists the nondimensional coordinates of the off-design inlet from the centerbody tip downstream to the compressor face. The cowl entrance diameter, 21.87 centimeters, is the same as that of the 60-40 inlet.

The inlet contours of the transonic 30-70 inlet were obtained by modifying a single-cone (10.5°) inlet designed for a Mach number of 2.7 (ref. 5). The area contraction of a capture stream tube of the inlet at the design Mach number of 2.7 was 30 percent external and 70 percent internal. To help eliminate the internal contraction of the off-design inlet, the cowl side of the internal flow passage was modified to increase the local flow area (fig. 1(c)). In addition, the centerbody was translated forward 0.6249 cowl diameter to remove the remaining internal contraction. The surface coordinates and the area variations of both the design and transonic versions of the 30-70 inlet are plotted in figure 1(c). Table I(c) lists the nondimensional coordinates of the off-design inlet from the centerbody tip downstream to the compressor face. The capture area of the inlet is 375.8 square centimeters. The cowl entrance diameter, 21.87 centimeters, is the same size as that of the two previously described inlets. Since the cowl diameter (and compressor face area) of the 30-70 inlet is identical in the present tests to that of the other two inlets, the 30-70 inlet is matched transonically as if it also were designed for Mach 2.5.

A schematic cross section of the model is presented in figure 2(a). With the exception of the model support sting, mass flow exit plug, outer shell windshield, and base pressure skirt, the entire model formed the metric unit of the force measuring system. The support sting and exit plug were completely grounded. The outer shell windshield and base pressure skirt were only grounded in the axial direction to allow free movement in the transverse direction. These nonmetric parts of the model are identified in the schematic presented in figure 2(a). The nonmetric outer shell windshield was used to reduce the friction drag over the aft part of the model. A bearing of 30 Teflon spacers was installed between the outer shield and the 25.4-centimeter metric cylinder. These triangular shaped spacers prevented the friction drag from being transferred to the metric cylinder (see fig. 2(b)). To prevent airflow between the two surfaces and a resulting friction drag, a neoprene curtain was installed in the annular passage between the two shells near the leading edge of the outer shell windshield.

The load cell was mounted between the centerbody and the model support sting (fig. 2(a)) and had a load capacity of ±4500 newtons. Since variation in perpendicular loads would affect the load cell reading, the load cell had to be isolated from all such forces. Both a sting bearing and a strut bearing (fig. 2(c)) were used to isolate the perpendicular loads on the load cell. If the strut bearing had not been used, the perpendicular design load of the sting bearing would have been exceeded. The side forces were eliminated by using the bearing parts of a separate strut balance system from which the strain gages were removed. This bearing system removed both vertical and horizontal forces so that only axial forces were actually applied to the load cell. The effectiveness of the bearing system was indicated by the result that the standard deviation of the data from a linear calibration curve was less than 0.9 newton. The axial loads used in determining drag were an average of 10 readings randomly taken over a period of roughly 2 seconds. This technique of data taking was necessitated by a condition of model vibration during testing and resulted in a typical standard deviation of 8 newtons for the 10 load cell measurements taken at each test point. Consequently, there was roughly a 68-percent chance that the recorded mean was within 2.5 newtons of the true value.

Two bypass door configurations were tested with all three inlets: (1) closed bypass doors, which are indicated by the dotted line in figure 3(a), and (2) 5° open multiple-flap bypass doors (fig. 3(a)). In addition, a third door configuration was tested with the 60-40 inlet: 10° open multiple-flap bypass doors (fig. 3(a)). The flow passage between each of the flaps had side plates so that the bypass flow could be ejected in a downstream direction. The flap contour is depicted in detail in figure 3(b). The general location of the door with respect to the inlet can be seen in the model schematic of figure 2(a), which depicts the multiple-flap bypass door configuration. A photograph of the 5° multiple-flap bypass doors is shown in figure 4.

Instrumentation

The pressure measurement instrumentation included an axial row of static-pressure taps along the centerbody at 90° and along the top (0°) external surface of the cowl. The locations of these static-pressure taps are listed in table II, and their relative positioning on the inlet is shown in figure 5(a). The total- and static-pressure instrumentation located at the compressor face station is depicted in figure 5(b). There were five six-tube total-pressure rakes, one four-tube dynamic pressure rake, and nine wall static-pressure taps at this model station. There were total-pressure rakes located both at the same circumferential angle as the centerline of the bypass doors and at the same angle as the midway point between the bypass doors (fig. 5(b)). These doors were just upstream of the rakes (fig. 2). Total pressures were measured at the cowl lip station with a single rake, as depicted in figure 5(c). The total-pressure tubes in the rakes at both the cowl lip and the compressor face were area weighted. The average total pressures that are presented in this report are the area-weighted averages of total pressures at a particular rake station. The steady-state distortion is the quotient $(P_{max} - P_{min})/\overline{P}_2$. Since flow symmetry at the compressor face was assumed, only one-half of the compressor face plane was instrumented. Calculations of pressure recovery and distortion at the compressor face were based on this assumption. In addition, static pressures were measured in the cold pipe just upstream of the mass flow plug and were used in conjunction with the exit area to calculate mass flow. Base static pressures and load cell chamber pressures were also measured in order to calculate tare loads (see appendix B). The definition of the drag terms along with the equations used to obtain the additive and total inlet drag from measured quantities are also presented in appendix B.

The dynamic pressures were recorded with subminiature strain-gage pressure transducers whose output was filtered by a 2-kilohertz low pass filter and then fed into the root-mean-square meters. The value of compressor face dynamic distortion presented in this report is the average of the four dynamic (root-mean-square) total pressures divided by the average of the 30 steady-state total pressures. The bypass mass flow ratio m_{bp}/m_0 was obtained by subtracting the compressor face mass flow ratio measured at a particular open bypass condition from that measured with the bypass doors closed at the identical entrance Mach number M_1.

Procedure

The testing was divided into two parts; the first was primarily concerned with the bulk of the pressure measurements, and the second was primarily concerned with the force measurements. Duplicate runs were made for each bypass door configuration, and the measurements were correlated by the measured mass flow at the exit plug. Conse-

quently, to compare the drag and performance of one inlet configuration with another, it was necessary first to plot the data against mass flow m_3/m_0 in order to obtain identical test conditions.

The Mach numbers tested were nominally 0.8, 0.9, 1.0, 1.1, 1.2, and 1.27. The associated Reynolds numbers were 1.38×10^7, 1.41×10^7, 1.46×10^7, 1.51×10^7, 1.54×10^7, and 1.54×10^7 per meter, respectively. The three inlets were tested at zero angle of attack at all six Mach numbers and, in addition, at angles of attack of 2°, 5°, and 10° at Mach 1.27. The engine demand corrected weight flow schedule used is presented in figure 6. The experimental mass flow ratios corresponding to the design corrected weight flow of each inlet configuration tested are shown in table III. These mass flow ratios were determined by matching a GE 4 engine to each inlet at the design Mach number and determining the resulting inlet-engine match at transonic speeds.

RESULTS AND DISCUSSION

Inlet Performance

It is possible to know how the different inlets should operate by looking at figure 1. The 60-40, 40-60, and 30-70 inlets have minimum throat areas of 0.755, 0.760, and 0.680 of the capture area, respectively. Therefore, near Mach 1, the throats should choke at mass flow ratios approximately equal to these ratios of throat to capture area. The important operating inlet mass flow ratios are presented in table III for the "matched" engine corrected weight flow. At Mach 1, the engine mass flow ratio is about 0.63 to 0.65 for all the inlets with the bypass closed. Opening the bypass to 5° dumps mass flow equivalent to a mass flow ratio of at least 0.06, and opening the bypass to 10° lowers the mass flow ratio about 0.10. Therefore, adding the 0.06 bypass mass flow ratio to the 0.63 engine mass flow ratio gives 0.69, which exceeds the throat to capture ratio of the 30-70 inlet so that it should be operating supercritically with the bypass open. However, the larger throat to capture area of the other two inlets would prevent supercritical operation until the doors are opened to at least 10°, where the sum of the engine and bypass mass flows would equal the throat to capture area ratio. Similar effects would be expected at other Mach numbers.

The other inlet characteristic that can be discerned from figure 1 is the mass flow spillage characteristic. The lack of any internal contraction for the 30-70 inlet implies it will accept all of the cowl lip flow if the inlet is operated supercritically. This would avoid spilling of flow behind an external normal shock, which would normally cause high drag. However, the 60-40 inlet flow area contracts from 0.845 of the capture area at the cowl lip to 0.755 internally. Therefore, even with the internal area choked, mass flow equivalent to a mass flow ratio of 0.09 would have to be spilled over the cowl behind

a normal shock. The 40-60 inlet would similarly have to spill mass flow equivalent to a 0.03 mass flow ratio.

Performance at matched conditions for the various inlets as a function of free-stream Mach number is presented in figure 7. The dynamic distortion, steady-state distortion, and total-pressure recovery are presented for the transonic 40-60 and 30-70 inlets for closed and 5° bypass door configurations and for the 60-40 inlet for closed, 5°, and 10° bypass door configurations. The experimental data are presented as a function of mass flow ratio in figures 18 to 23, which are included for reference only. The data of figure 7 were obtained by entering the curves of figures 18 to 23 at the mass-flow ratio shown in table III which corresponded to the design corrected weight flow. The total-pressure recovery between the Mach numbers of 0.8 and 1.27 was between 0.98 and 0.99 for the 60-40 and 40-60 inlets for the closed and 5° bypass door configurations. Since the total-pressure recovery was low and the distortion was high with the 60-40 inlet with the 10°-bypass door configuration, the inlet was undoubtedly operating with a choked throat and a resulting terminal shock in the subsonic diffuser. The total-pressure recovery of the 30-70 inlet was lower than the recovery of the other two inlets for all bypass configurations tested. For the 5° bypass door configuration, supercritical inlet operation reduced the recovery considerably over the entire Mach number range tested. At Mach 1.27 the potential total-pressure recovery was reduced by the higher normal shock losses associated with the high Mach number on the exposed centerbody shoulder. Even at Mach 0.8 the flow over the 30-70 inlet accelerated to sonic or near sonic values on the external surface of the cone. For most of the inlets and Mach numbers tested, the steady-state distortion was below 0.10 and the dynamic distortion was below 0.010 for subcritical operation. The 30-70 inlet did have higher values of distortion, especially with the 5° bypass door configuration; this difference was probably due to the higher Mach number on the exposed centerbody shoulder and the smaller throat.

Performance as a function of angle of attack at a free-stream Mach number of 1.27, design corrected weight flow, and closed and 5° bypass flap door configurations is presented in figure 8. For the 40-60 and 60-40 inlets the pressure recovery with the closed door configuration was more sensitive to angle of attack than with the bypass flaps set at 5°. This sensitivity generally resulted in the 5° flaps giving better performance at angle of attack than the closed door configuration. Because the 30-70 inlet operated supercritically at the design corrected weight flow when the bypass flaps were set at 5°, the closed door configuration provided better performance over the entire range of angle of attack ($0^{\circ} < \alpha \leq 10^{\circ}$). The steady-state distortion of both the 40-60 and 60-40 inlets was roughly the same.

The radial variations of the dynamic and total pressures of the 60-40, 40-60, and 30-70 inlets are presented in figures 9 to 11 for Mach numbers of 1.27, 1.0, and 0.8. Large values of dynamic distortion near the centerbody and cowl were accompanied by steep gradients in total-pressure recovery at these locations. This characteristic was

exhibited at all three free-stream Mach numbers. As depicted in figures 9 and 10, low-energy boundary-layer air was removed from the cowl side of the duct as the bypass flaps were opened. The trend was not observed with the 30-70 inlet (fig. 11) because of its supercritical operation when the bypass flaps were set at 5°. The change in inlet operation was so drastic that the cowl side boundary-layer removal effect was masked. When the bypass flaps were opened to 10° on the 60-40 inlet, enough air passed through the inlet to choke the throat flow. The increased throat Mach number at larger bypass flow resulted in additional pressure losses, indicated by lower pressure recoveries in figure 9 at $M_0 = 1.27$ and 1.0. Dynamic distortion was generally low for the 60-40 and 40-60 inlets (0.01 or less) when the bypass was closed. Slight increases in dynamic distortion occurred with bypass flow. The 30-70 inlet exhibited higher dynamic distortion than the other two inlets with the bypass closed. Even higher values of distortion were recorded for the 30-70 inlet with the bypass open.

Inlet Drag

The total inlet drag as derived from model balance measurements and equation (B1) (appendix B) varied greatly between the inlets at similar bypass flap angles and free-stream Mach numbers. The effects of these variations are presented in figure 12. For each inlet tested there was a transonic drag rise that began between Mach 0.9 and 1.05 and ended between Mach 1.0 and 1.2. However, the magnitude of the rise varied considerably from inlet to inlet with the largest value for the 60-40 inlet and the smallest for the 30-70 inlet. The drag rise decreased as more flow was spilled by the centerbody. The centerbody area at the cowl lip is equal to $1 - A_1/A_0$, where A_1/A_0 is the annular flow area at the cowl lip. Figure 1 shows this ratio to be 0.68, 0.79, and 0.84 for the 30-70, 40-60, and 60-40 inlets, respectively, values giving centerbody area ratios of 0.32, 0.21, and 0.16, respectively. The relation between the cone cross-sectional areas and drag is due to the fact that supersonic spillage generated by the cone provides much lower drag than subsonic spillage from behind a normal shock.

The rise in transonic total drag coefficient for the 60-40 inlet with closed bypass doors was roughly 0.18. When the bypass doors were opened to a flap angle of 5°, the drag rise was reduced to 0.12 primarily because of less bow shock spillage at the higher Mach numbers. At Mach 0.8 and 0.9 the value of the drag coefficient was increased by dumping flow through the bypass doors. The net sum of these two effects at Mach 1.2 and 1.27 was to yield a lower drag with mass flow spilled through bypass doors than with all the excess mass flow spilled over the cowl. The crossover for the total drag curves of the two bypass configurations was at about Mach 1.09. Consequently, below Mach 1.09 it was better to spill flow over the cowl of the 60-40 inlet than through the bypass doors, and above Mach 1.09 it was better to spill flow through the bypass doors. The

general character of the drag coefficient of the 40-60 inlet differed from that of the 60-40 inlet since the drag at low Mach numbers was lower with the bypass doors open than with them closed. This difference was probably associated with the different cowl drags measured with each inlet.

The transonic 30-70 inlet generally had a lower total drag than the 60-40 and 40-60 inlets. At a flap angle set at 5° and at supersonic free-stream Mach numbers the 30-70 inlet operated supercritically and consequently should not be compared with any other bypass flap configuration. Similar trends can be seen in figure 13.

Drag Breakdown

Figure 14 presents the additive drag as a function of inlet mass flow for the various inlets operating at the six Mach numbers. There are sections of each curve which are two overlapping sets of data, one obtained from high bypass spillage and the other from lower bypass spillage. At these overlapped conditions the data could always be plotted on a smooth curve which was a function of only inlet mass flow ratio m_1/m_0. The additive drag was obtained from the integration of the centerbody pressures and from the difference in flow impulse between the cowl lip station and the free stream. At all test mass flow ratios and Mach numbers the list of inlets in order of increasing additive drag was 30-70, 40-60, and 60-40. The additive drag of the 30-70 inlet was considerably less than those of the other inlets tested because of the larger centerbody spillage. This low additive drag was responsible for the drag of the 30-70 inlet being the lowest. The drags of the other two inlets were close together with a spread in drag coefficient no greater than 0.045 and an average spread of approximately 0.035; the 60-40 inlet always had the larger drag of the two.

The cowl pressure drags presented in figure 15 were obtained by integrating the cowl pressures. Again two overlapping sets of data, one obtained from high bypass spillage and the other from lower bypass spillage, could always be plotted on a smooth curve which was a function of only inlet mass flow ratio m_1/m_0. The 40-60 and 30-70 inlets had identical cowls with a 3° initial external angle, while the 60-40 inlet cowl had an initial external angle of 8°. At all test mass flow ratios and Mach numbers the list of inlets in order of decreasing cowl suction forces (increasing cowl drag) was 60-40, 40-60, and 30-70. Also, at subsonic Mach numbers, the slope of the 60-40 curve was greater than that of the other two inlets, which indicated that this inlet with the high lip angle was recovering more additive drag (because of cowl lip suction) per unit of spillage mass flow than the other inlets. This was the primary reason why the 60-40 inlet at subsonic speeds had less total drag with the bypass closed than with the bypass open (fig. 12).

The sum of the cowl and additive drags, the partial inlet drag, is presented in figure 16. At Mach 0.8 and high mass flow ratios the partial inlet drag of all the inlets was zero or less, and consequently the additive drags were totally recovered by lip suction forces associated with these cowls. The additive drag was also recovered at Mach 0.9 for the 30-70 inlet. At higher Mach numbers it was more difficult for the flow to expand around the sharp edge of the cowl lip. As the Mach number increased, the flow was more likely to separate on the free-stream side of the cowl; the result was a higher pressure than if there were no separation. Thus, at supersonic speeds it was best to spill excess air with a large centerbody. Since the cowl lip forces were much less, any air that needed to be dumped in addition to the supercritical mass flow spillage was best taken on board and spilled through the bypass independently of the cowl lip shape. Subsonically (in the range studied), it was best to spill the remainder of the excess airflow over the cowl of inlets with a high lip angle so that the larger cowl lip suction forces would recover a higher fraction of the additive drag.

The important pressure measurements that determine the cowl and additive drag are static pressures on both the external centerbody and cowl surfaces. Typical cowl and centerbody static pressures are presented in figure 17. The external cowl surface of the 60-40 inlet consists of two conical sections with a sharp break at a model station of roughly 1.39. This discontinuity in the slope of the surface resulted in the sharp decrease in pressure shown in figure 17(a-1). The break in the surface of the 40-60 and 30-70 inlets is much less (0.4°) than that of the 60-40 inlet and consequently resulted in a smoother pressure variation along the cowl, as depicted in figures 17(a-2) and (a-3).

For comparison figure 17(a), at $M_0 = 1.27$, shows a two-dimensional estimate of the expected cowl pressure in the conical flow field for a fully flowing inlet with no bow shock or cowl separation. For the 60-40 and 40-60 inlets, where considerable flow was spilled behind a normal shock, pressures considerably below the predicted value were obtained. These low pressures were representative of cowl lip suction, which partially offset the higher additive drag. The good agreement between predicted and measured pressures for the 30-70 inlet corresponded to the lack of subcritical spillage for the inlet. The pressure distribution on the 10° cone surface of the 60-40 inlet (fig. 17(a-1)) indicated the static pressures were greater than that from a simple normal shock. This increased pressure originated from the added diffusion associated with air spilled over the cowl by the normal shock. Since less air was ingested, the entrance Mach number decreased and the static pressure at the entrance increased. Near the cowl lip station the pressures decreased as more air was dumped overboard through the bypass doors, since the entrance Mach number was increasing to accommodate the additional mass flow. Concomitantly, the normal shock moved downstream toward the cowl lip as more air was ingested. The ingested mass flow increased as the mass flow plug opened until the throat flow choked at some particular location of the external bow shock. At this choked flow condition the performance of the inlet was similar to that of a started inlet

operating supercritically with an internal diffuser normal shock in addition to a bow shock and with the total-pressure recovery decreasing at constant inlet mass flow. The pressure distributions at Mach 1.0 and 0.8 are presented in figures 17(b-1) and (c-1). The pressures at these Mach numbers exhibited the same characteristic as existed behind the bow shock at Mach 1.27. With no bypass mass flow dump the cone pressures were higher at the cowl lip face station than with the bypass, which indicated a lower Mach number and decreased ingested mass flow. The cone static pressures of the 40-60 inlet were similar to those of the 60-40 inlet.

Because the minimum flow area was located at the cowl lip station, the cone static pressures of the 30-70 inlet were considerably different from the static pressures of the 60-40 and 40-60 inlets. The absence of the constraint of a choked throat permitted the external normal shock to be swallowed by the inlet. Static-pressure data indicated that the 30-70 inlet was operating supercritically at all supersonic design conditions with the bypass flap angles set at 5°. At Mach 1.27 with no bypass flow a bow shock existed at the design engine corrected weight flow. The peak external cone pressure (fig. 17(a-3)) indicated that the local Mach number was near 1 and that there was very little mass flow spillage behind the bow shock at this condition. When the bypass doors were opened, the bow shock fell back and was ingested by the inlet. The cone static pressures decreased near the cowl lip station as the bow shock moved downstream to the inside of the inlet. The pressure decrease indicated the existence of a local cone surface Mach number greater than the free-stream Mach number. With no bypass the cone Mach numbers overexpanded to 1.32 and at the 5° bypass flap setting to 1.43.

SUMMARY OF RESULTS

The transonic performance, including both pressure and drag data, of three supersonic inlets was determined over a Mach number range of 0.8 to 1.27. The Reynolds number of the three axisymmetric models varied from 1.38×10^{7} to 1.54×10^{7} per meter depending upon Mach number. All the inlets were designed by scaling the dimensions of inlets designed for supersonic cruise. Transonic configurations were derived by collapsing various surfaces or translating the centerbody of the scaled down inlet or both. Pressure and drag measurements allowed the drag to be broken down into additive, cowl, and total inlet drag. The following results were obtained from the test:

1. At a Mach number of 0.8 the inlet drag of the 60-40 and 30-70 inlets decreased when the bypass doors were closed and the excess airflow was spilled over the cowl.

2. At a Mach number of 1.27 the inlet drag of the 60-40 and 40-60 inlets was lowest when the bypass doors were partially open in order to spill ingested air.

3. Throughout the Mach number range tested, the 30-70 inlet consistently had the lowest drag. However, the 30-70 inlet also had lower pressure recoveries and higher distortions than the other inlets.

Lewis Research Center,
National Aeronautics and Space Administration,
Cleveland, Ohio, December 13, 1974,
505-04.

APPENDIX A

SYMBOLS

A	cross-sectional area, cm^2
A_c	capture area, cm^2
C_{DA}	additive drag coefficient, $drag/q_0A_c$
C_{DC}	cowl drag coefficient, $drag/q_0A_c$
C_{DT}	total inlet drag coefficient, $drag/q_0A_c$
D_c	diameter of cowl lip, 21.87 cm (8.612 in.)
F_{lc}	force measured on load cell, N
h	distance from centerbody surface, cm
I	impulse function, $pA + p\gamma AM^2$, N
M	Mach number
m	mass flow, kg/sec
P	total pressure, N/m^2
ΔP	$P_{max} - P_{min}$, N/m^2
P_{max}	maximum total pressure at compressor face station, N/m^2
P_{min}	minimum total pressure at compressor face station, N/m^2
P_{rms}	root mean square of instantaneous pressure, N/m^2
$\bar{P}_2$	average total pressure at compressor face station, N/m^2
p	static pressure, N/m^2
q	dynamic pressure, $\gamma pM^2/2$, N/m^2
R	radius, cm
ΔR	local duct height, cm
$w\sqrt{\theta}/\delta A$	corrected weight flow, $kg/(sec)(m^2)$
X	axial distance from spike tip, cm
Z	axial distance from cowl tip, cm
α	angle of attack, deg

Subscripts:

bp bypass

0 free stream

1 cowl lip

2 compressor face

3 mass flow measuring station

APPENDIX B

DRAG CALCULATIONS

The sketch in this appendix represents two different spillage configurations. One configuration uses the multiple-flap bypass door, where the inlet captures a free-stream tube of air with a cross-sectional area $A_{0,bp}$. Since the engine is designed to accept only an $A_{0,3}$ free-stream tube, the difference $A_{0,bp} - A_{0,3}$ is dumped out the bypass doors. The dots in the sketch denote the dump airstream tube. The other spillage configuration uses a closed bypass. The capture free-stream tube is represented by $A_{0,3}$. The dashed line traces this stream tube through the inlet.

The sketch depicts a decrease in additive drag, because of a decrease in frontal area of the free-stream capture tube whenever the bypass doors are open. There will be a penalty, however, associated with the bypass dumping of the air which is related to the nozzle efficiency of the doors.

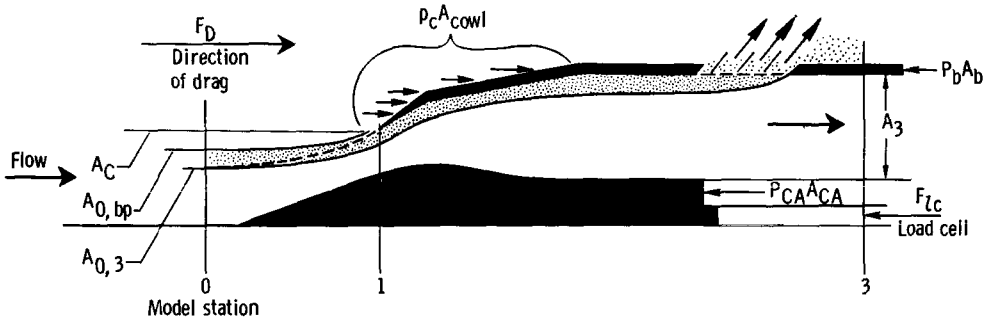

The various drag terms used in the report were calculated by using the following expressions:

$$F_A = (I_1 - I_0) + \sum p_{cone}\, \Delta A_{cone} - p_0(A_c - A_{0,bp})$$

$$F_C = \sum p_c\, \Delta A_{cowl}$$

$$F_F = C_f S_f q_0$$

where

$$C_f = f(M_0)$$

(ref. 6) and S_f is the external wetted flow area.

$$F_T = F_{lc} + I_3 - I_0 + p_b A_b + p_{CA} A_{CA} - p_0(A_b + A_{CA} + A_3 - A_{0,bp}) \tag{B1}$$

where

$$I_0 = 2q_0 A_{0,bp} + p_0 A_{0,bp}$$

$$I_1 = p_1(A_c - A_{cone}) + \gamma p_1 M_1^2 (A_c - A_{cone})$$

$$I_3 = p_3 A_3 + \gamma M_3^2 p_3 A_3$$

$$A_{0,bp} = A_c \frac{m_1}{m_0}$$

and

F_A additive drag

F_C cowl drag

F_F friction drag

F_T total inlet drag

I impulse function

with the subscripts

cone cone

cowl cowl

b base

CA cavity

The actual drag coefficients were obtained by dividing the previously listed drags by $q_0 A_c$.

REFERENCES

1. Koenig, Robert W.: Inlet Sensitivity Study for a Supersonic Transport. NASA TN D-3881, 1967, pp. 20-21.

2. Neale, M C.; and Armstrong, F. W.: Some Recent Research on Supersonic Intakes at NGTE. Aerodynamic Interference. AGARD-CP-71-71, Advisory Group for Aerospace Research and Development, 1971, pp. 19-1 to 19-16.

3. Wasserbauer, Joseph F.; and Choby, David A.: Mach 2.5 Performance of a Biconic Inlet With Internal Focused Compression and 40-Percent Internal Contraction. NASA TM X-2294, 1971.

4. Cubbison, Robert W.; Meleason, Edward T.; and Johnson, David F.: Performance Characteristics From Mach 2.58 to 1.98 of an Axisymmetric Mixed-Compression Inlet System With 60-Percent Internal Contraction. NASA TM X-1739, 1969.

5. Syberg, J.; and Koncsek, J. L.: Transonic and Supersonic Test of the SST Prototype Air Intake. FAA-SS-72-50, Federal Aviation Administration, 1972. (Available from DDC as AD-894459.)

6. Woollett, Richard R.; Meleason, Edward T.; and Choby, David A.: Transonic Off-Design Drag and Performance of an Axisymmetric Inlet With 40-Percent Internal Contraction on Design. NASA TM X-3042, 1974.

TABLE I. - INLET COORDINATES

(a) 60-40 Inlet; lip station 1.0943

Centerbody		Cowl, internal		Cowl, internal	
X/D_c	R/D_c	Z/D_c	R/D_c	Z/D_c	R/D_c
0.0000	0.0000	0.0000	[a]0.5000	1.4644	0.5022
.2322	.0409	.0448	.5039	1.5030	.5051
1.4145	.2494	.1029	.5086	1.5631	.5098
1.4293	.2520	.1609	.5127	1.6191	.5135
1.4873	.2629	.2190	.5159	1.7353	.5174
1.5454	.2697	.2771	.5182	1.8514	.5195
1.6035	.2717	.3351	.5193	1.9675	.5207
1.6615	.2697	.3932	.5188	2.0466	.5214
1.7196	.2679	.4512	.5172	2.0836	.5217
1.7776	.2661	.5093	.5152	2.2175	.5225
1.8357	.2642	.5673	.5136	2.4497	.5208
1.8938	.2610	.6254	.5122	2.5658	.5179
1.9518	.2563	.6835	.5107	2.6820	.5153
2.0099	.2490	.7415	.5091	2.7400	.5142
2.0679	.2414	.7996	.5072	2.7981	.5135
2.1260	.2327	.8576	.5049	2.8045	.5134
2.1840	.2253	.9157	.5020	2.9206	.5134
2.2421	.2182	.9738	.4993	Cowl, external	
2.3002	.2120	1.0318	.4971	Z/D_c	R/D_c
2.3582	.2058	1.0899	.4957	0.000	[a]0.5023
2.4163	.1998	1.1479	.4951	.3140	.5464
2.4743	.1962	1.2060	.4949	1.4644	.5806
2.5324	.1931	1.2641	.4951		
2.5586	.1916	1.3221	.4962		
3.8986	.258	1.3802	.4981		
		1.4382	.5008		

[a]Lip radius, 2.54×10^{-2} cm.

(b) 40-60 Inlet; lip station 1.0179

Centerbody		Cowl, internal		Cowl, internal	
X/D_c	R/D_c	Z/D_c	R/D_c	Z/D_c	R/D_c
0.0000	0.0000	0.3107	0.4986	1.7264	0.5098
.2322	.0514	.3645	.4971	1.7875	.5135
1.0505	.2322	.4181	.4950	1.8986	.5174
1.1748	.2270	.4374	.4942	2.0147	.5195
1.2909	.2224	.4718	.4925	2.1309	.5207
1.4070	.2177	.5254	.4894	2.2099	.5214
1.5231	.2116	.5792	.4861	2.2470	.5217
1.6392	.1965	.6060	.4843	2.3809	.5225
1.6973	.1858	.6328	.4825	2.6131	.5208
1.7553	.1904	.6597	.4805	2.7292	.5179
1.8715	.1962	.6865	.4784	2.8453	.5153
1.9876	.2003	.7133	.4767	2.9034	.5142
2.1037	.2009	.7375	.4762	2.9614	.5135
2.2198	.1993	.7665	.4761	2.9678	.5134
2.3359	.1975	.7872	.4763	3.0840	.5134
2.4520	.1951	.8203	.4769	Cowl, external	
2.5682	.1930	.8739	.4779	Z/D_c	R/D_c
2.6425	.1916	.9275	.4789	0.0000	[a]0.5023
2.6456	.1916	.9813	.4799	.4783	.5274
3.9856	.2584	1.0350	.4808	1.6277	.5806
Cowl, internal		1.1422	.4829		
Z/D_c	R/D_c	1.2495	.4850		
0.0000	[a]0.5000	1.3569	.4883		
.2303	.5000	1.4342	.4914		
.2573	.4998	1.5622	.4979		
		1.6277	.5022		
		1.6663	.5051		

(c) 30-70 Inlet; lip station 1.7513; spike tip translation, 0.6249; cowl coordinates same as in (b)

Centerbody	
X/D_c	R/D_c
0.0000	0.0000
1.3856	.2526
1.4437	.2614
1.5598	.2731
1.6373	.2788
1.6759	.2807
1.7920	.2825
1.9082	.2801
2.0243	.2740
2.1404	.2646
2.2565	.2524
2.3726	.2386
2.7541	.1916
3.3790	.1916
4.719	.2584

TABLE II. - STATIC-PRESSURE-

TAP LOCATIONS

[Diameter of cowl lip D_c, 21.87 cm.]

Centerbody tap locations on 90° side centerline, X/D_c	Cowl tap locations on top centerline measured from cowl tip, Z/D_c
60-40 Inlet	
0.286	0.012
.496	.069
.640	.125
.757	.180
.858	.234
.949	.288
1.031	.342
[a]1.094	.413
	.483
	.608
	.802
	.993
	1.183
	1.371
40-60 Inlet	
0.262	0.023
.455	.067
.587	.111
.695	.155
.788	.286
.871	.415
.909	.553
.947	.701
.987	.847
1.017	.991
[a]1.0179	1.134
	1.275
	1.414
	1.552
30-70 Inlet	
0.651	(b)
.841	
.995	
1.128	
1.247	
1.356	
1.456	
1.544	
1.614	
1.684	
1.742	
[a]1.7513	

[a]Cowl station.

[b]Tap locations same as for 40-60 inlet.

TABLE III. - MASS FLOWS AT DESIGN

CORRECTED WEIGHT FLOW

(a) 60-40 Inlet

Free-stream Mach number, M_0	Bypass door flap angle, deg	Mass flow ratio		
		$m_1\ m_0$	$m_3\ m_0$	$m_{bp}\ m_0$
0.8	Doors closed	0.657	0.657	0.000
	5	.737	.657	.080
	10	.791	.654	.137
0.9	Doors closed	0.650	0.650	0.000
	5	.723	.649	.074
	10	.749	.636	.113
1.0	Doors closed	0.643	0.643	0.000
	5	.710	.643	.067
	10	.727	.625	.102
1.1	Doors closed	0.644	0.644	0.000
	5	.718	.645	.073
	10	.740	.620	.120
1.2	Doors closed	0.650	0.650	0.000
	5	.719	.646	.073
	10	.751	.627	.124
1.27	Doors closed	0.655	0.655	0.000
	5	.721	.651	.070
	10	.762	.635	.127

(b) 40-60 Inlet

0.8	Doors closed	0.659	0.659	0.000
	5	.733	.657	.076
0.9	Doors closed	0.649	0.649	0.000
	5	.720	.648	.072
1.0	Doors closed	0.642	0.642	0.000
	5	.713	.641	.072
1.1	Doors closed	0.643	0.643	0.000
	5	.718	.642	.076
1.2	Doors closed	0.647	0.647	0.000
	5	.720	.644	.076
1.27	Doors closed	0.650	0.650	0.000
	5	.710	.650	.060

(c) 30-70 Inlet

0.8	Doors closed	0.653	0.653	0.000
	5	.703	.641	.062
0.9	Doors closed	0.641	0.641	0.000
	5	.667	.608	.059
1.0	Doors closed	0.633	0.633	0.000
	5	.655	.590	.065
1.1	Doors closed	0.630	0.630	0.000
	5	.654	.584	.070
1.2	Doors closed	0.627	0.627	0.000
	5	.657	.580	.077
1.27	Doors closed	0.621	0.621	0.000
	5	.649	.573	.076

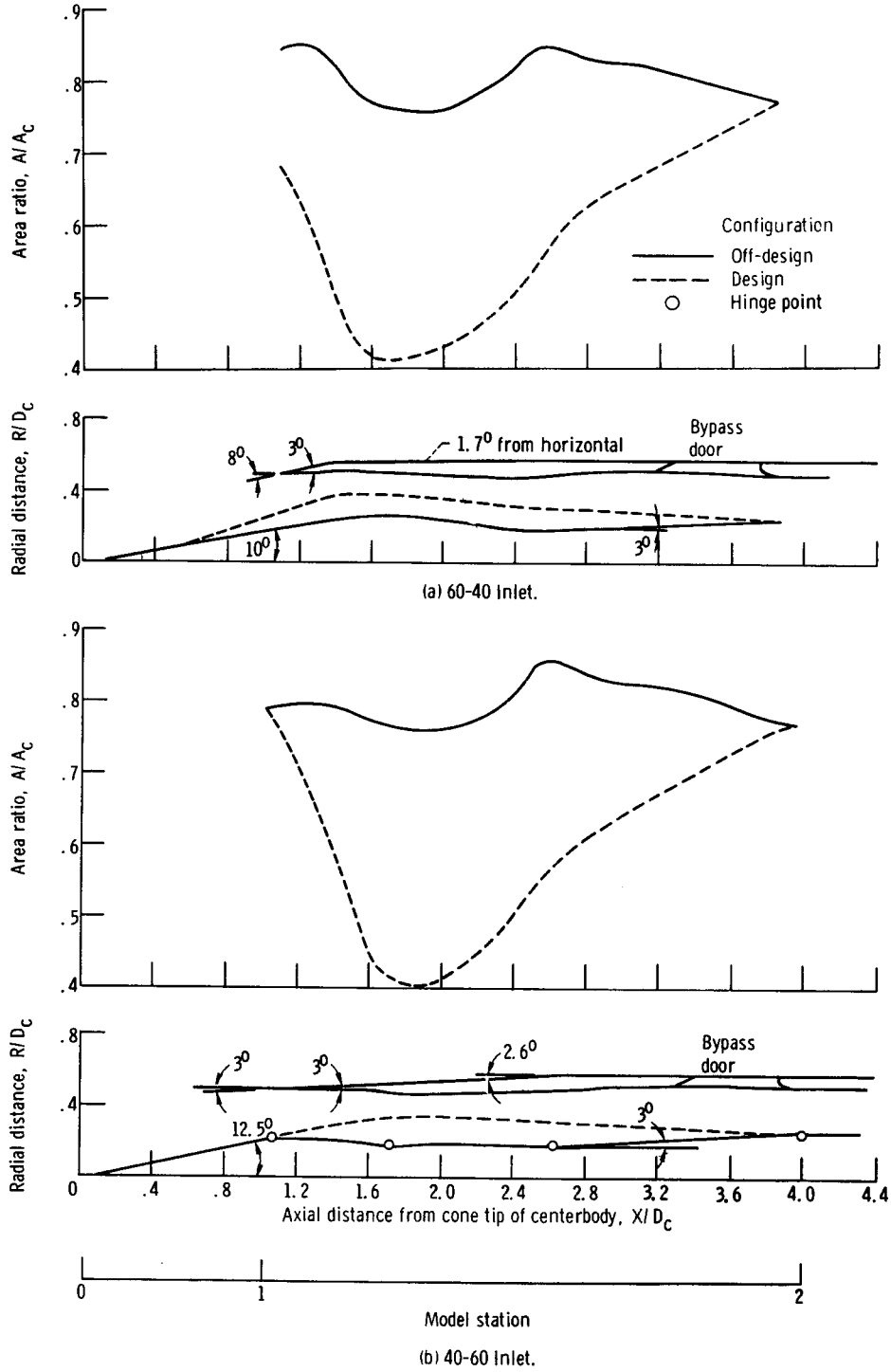

Figure 1. - Geometry of design and off-design configurations. Capture area, 375.8 square centimeters; diameter of cowl lip, 21.8 centimeters.

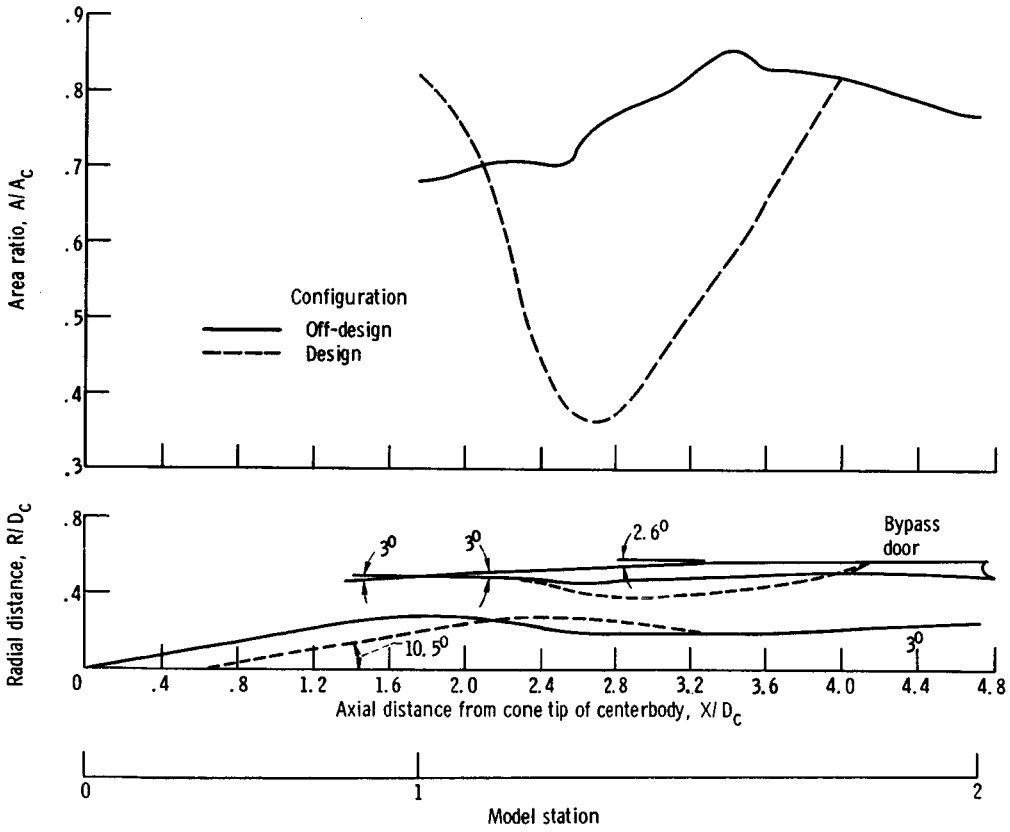

(c) 30-70 Inlet.

Figure 1. - Concluded.

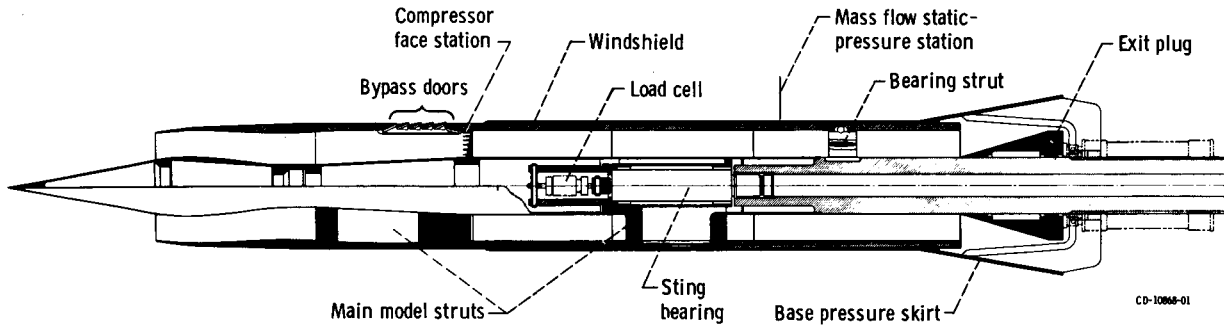

(a) Flow passages.

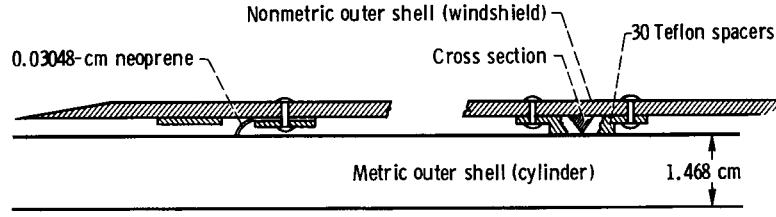

(b) Bearing surface between nonmetric outer shell (windshield) and 25.4-centimeter metric outer shell (cylinder).

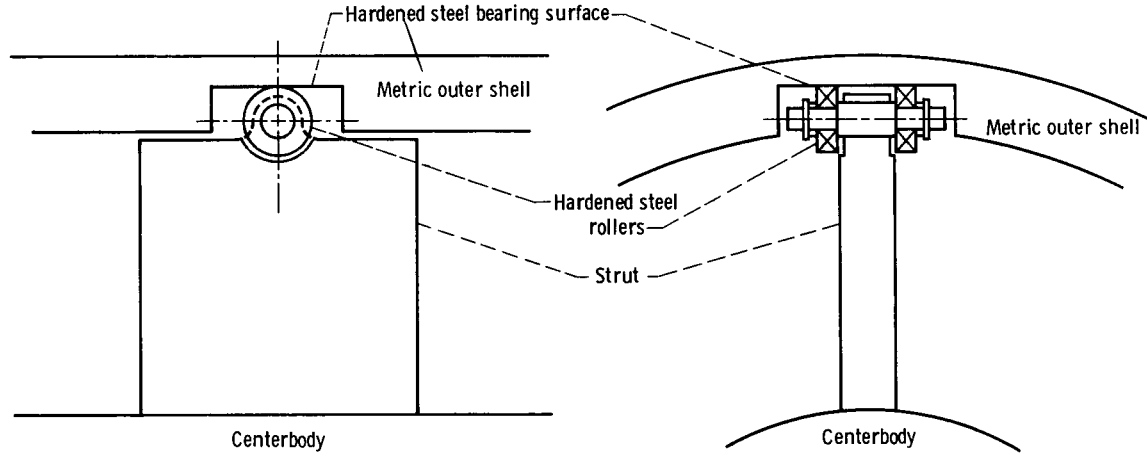

(c) Strut bearing; bearing shimed to allow 0.0127- to 0.0178-centimeter clearance with rollers.

Figure 2. - Schematic drawings of model.

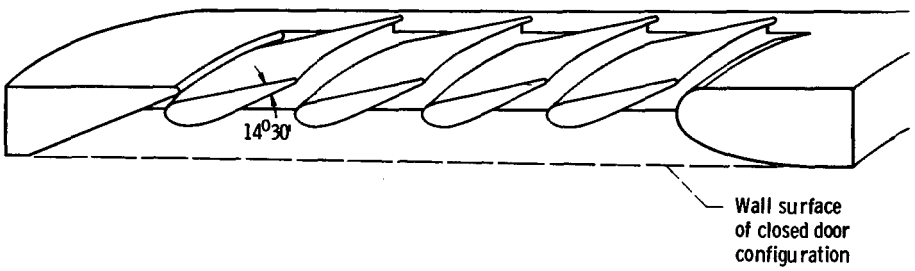

(a) Multiple flaps open 10°.

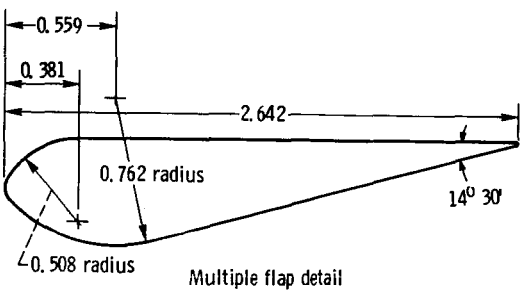

(b) Cross section of flap. Door width, 6.558 centimeters.

Figure 3. - Details of bypass door configuration. (All dimensions in centimeters unless otherwise noted.)

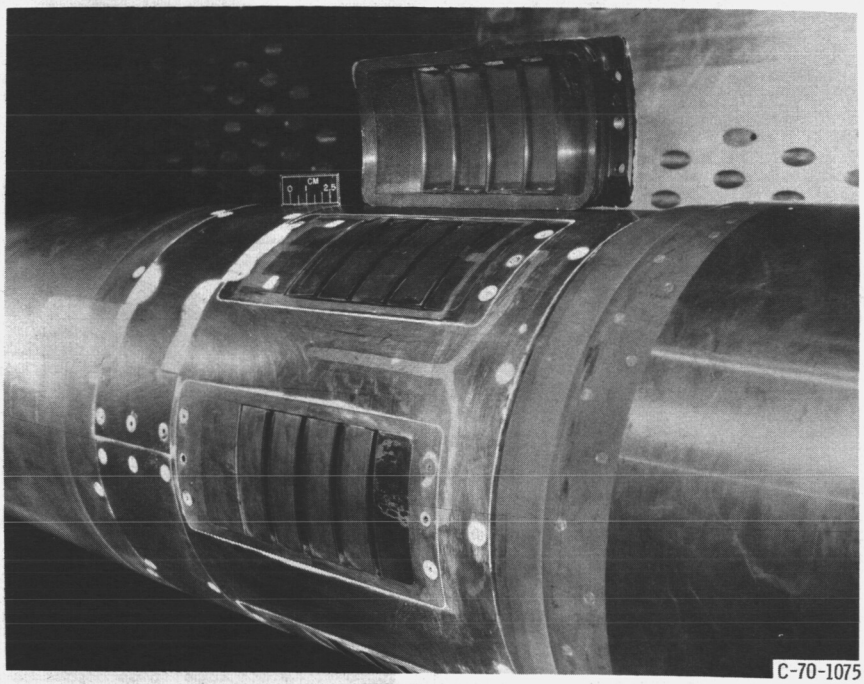

Figure 4. - View of 5° multiple-flap bypass doors looking upstream. On top of model is a spare multiple-flap door insert with underside in view.

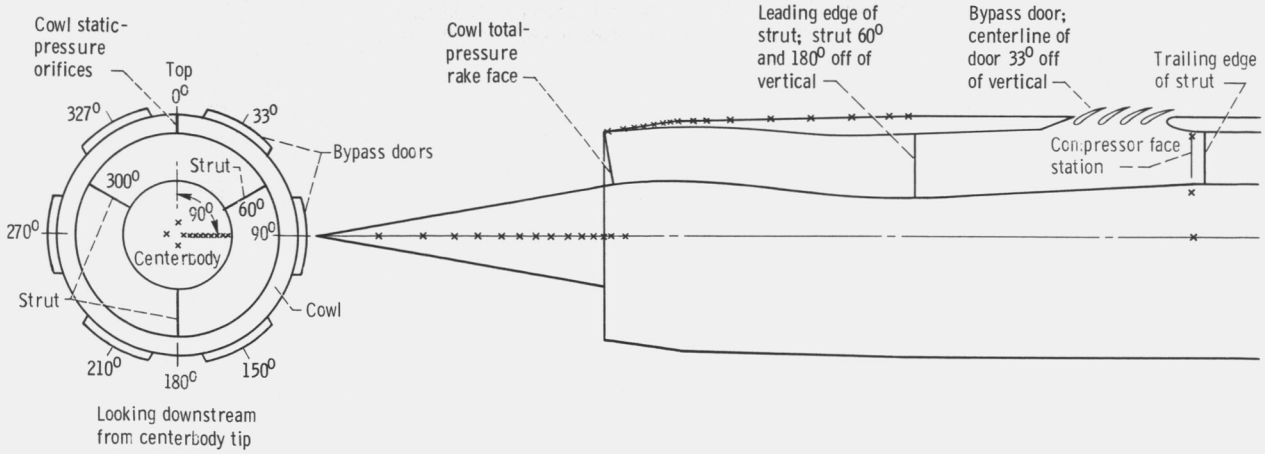

(a) Centerbody and cowl static- and total-pressure orifices.

Figure 5. - Model instrumentation.

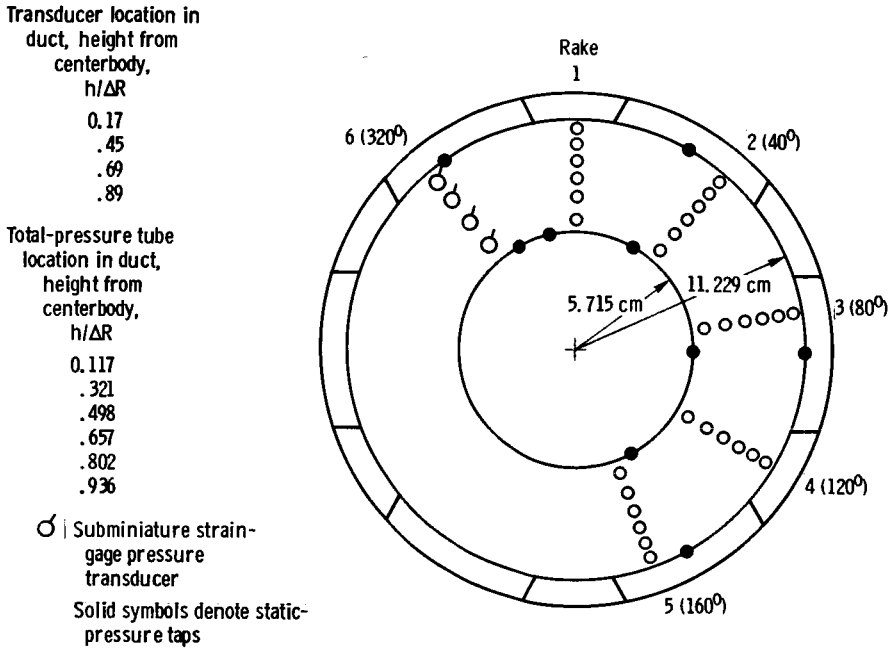

(b) Compressor face station instrumentation. Looking downstream at compressor face station (model station 2).

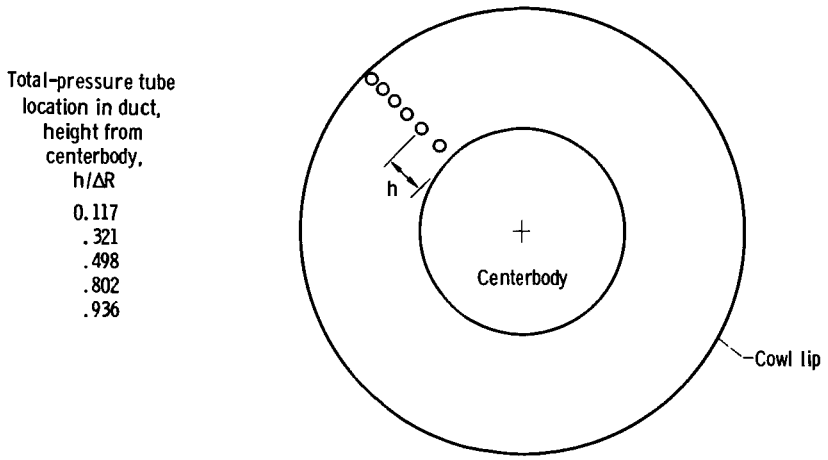

(c) Cowl face instrumentation. Looking downstream at cowl face rake (model station 1).

Figure 5. - Concluded.

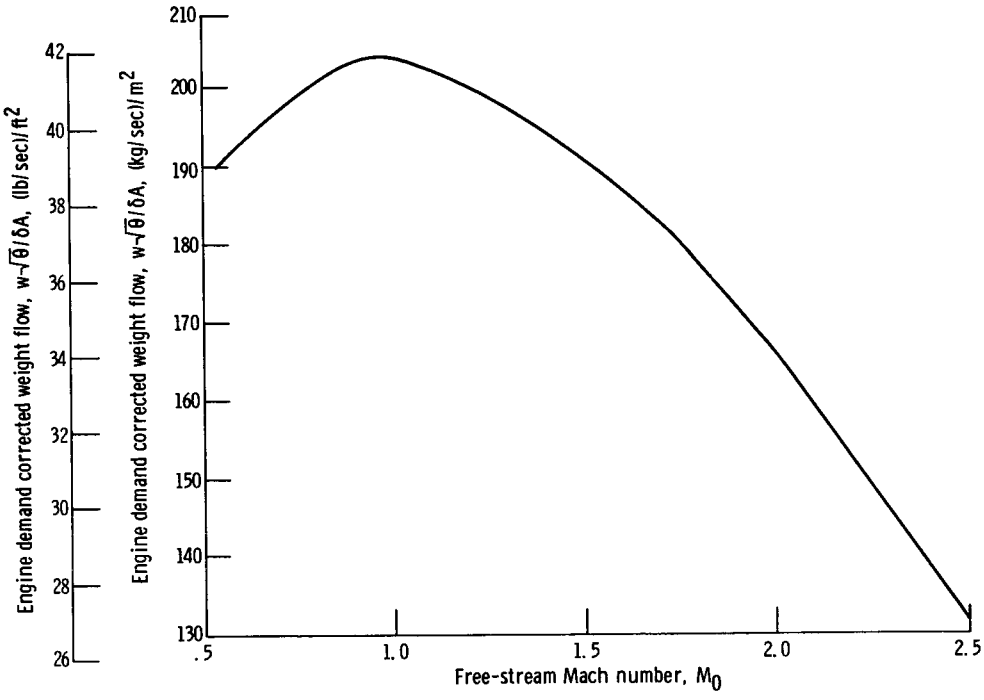

Figure 6. - Design corrected engine weight flow per unit area as function of Mach number.

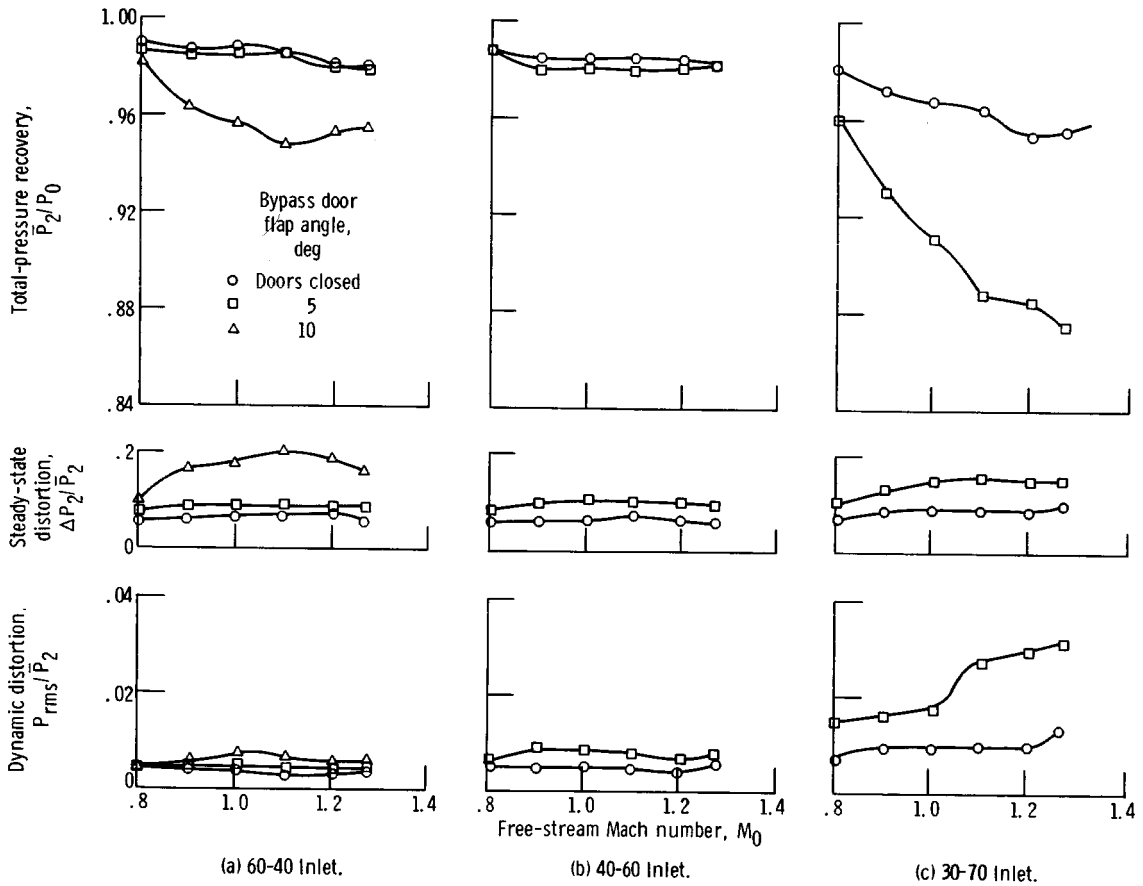

(a) 60-40 Inlet. (b) 40-60 Inlet. (c) 30-70 Inlet.

Figure 7. - Summary of performance of various inlets and bypass door configurations at design corrected weight flow and zero angle of attack.

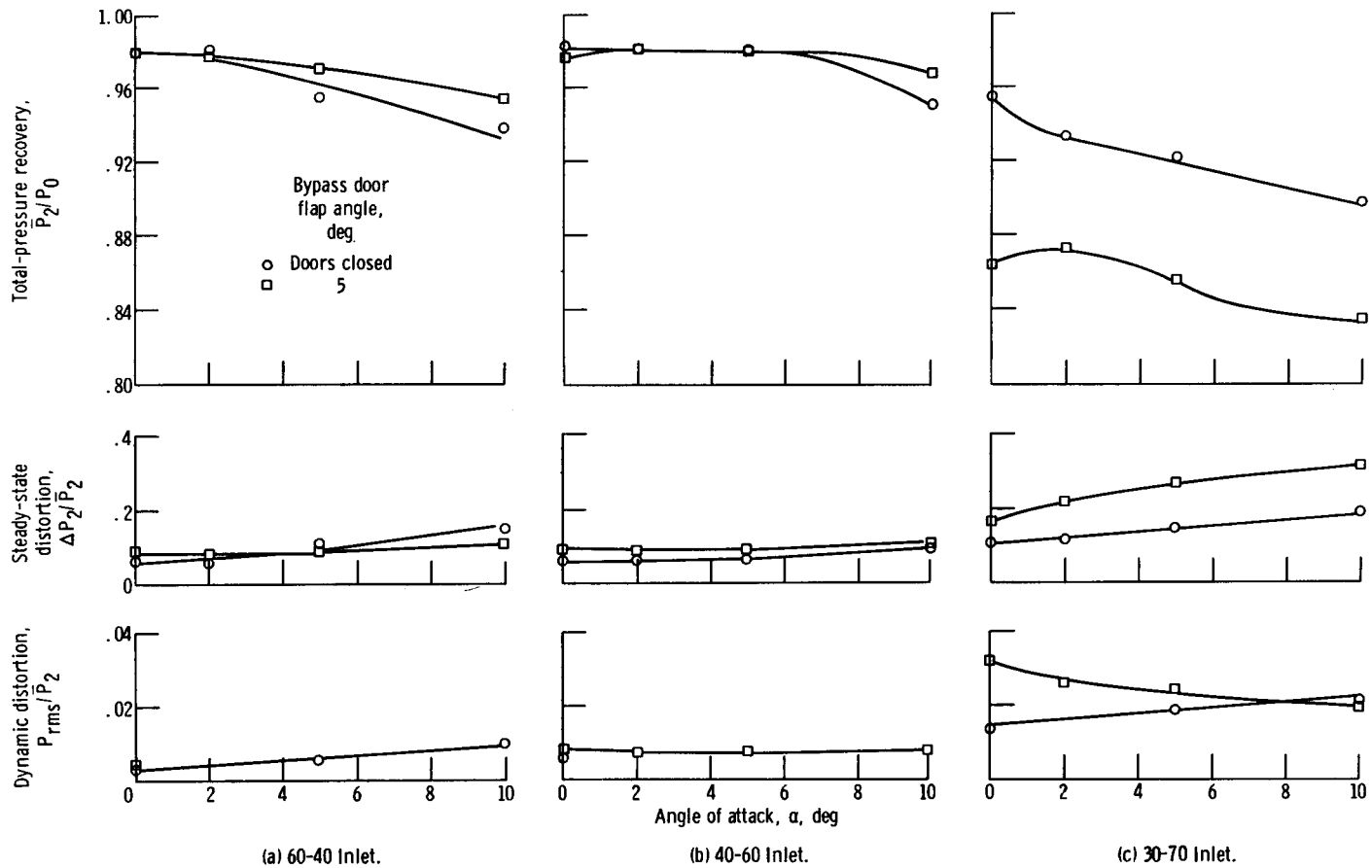

(a) 60-40 Inlet. (b) 40-60 Inlet. (c) 30-70 Inlet.

Figure 8. - Inlet performance as function of angle of attack at free-stream Mach number of 1.27 and design corrected weight flow.

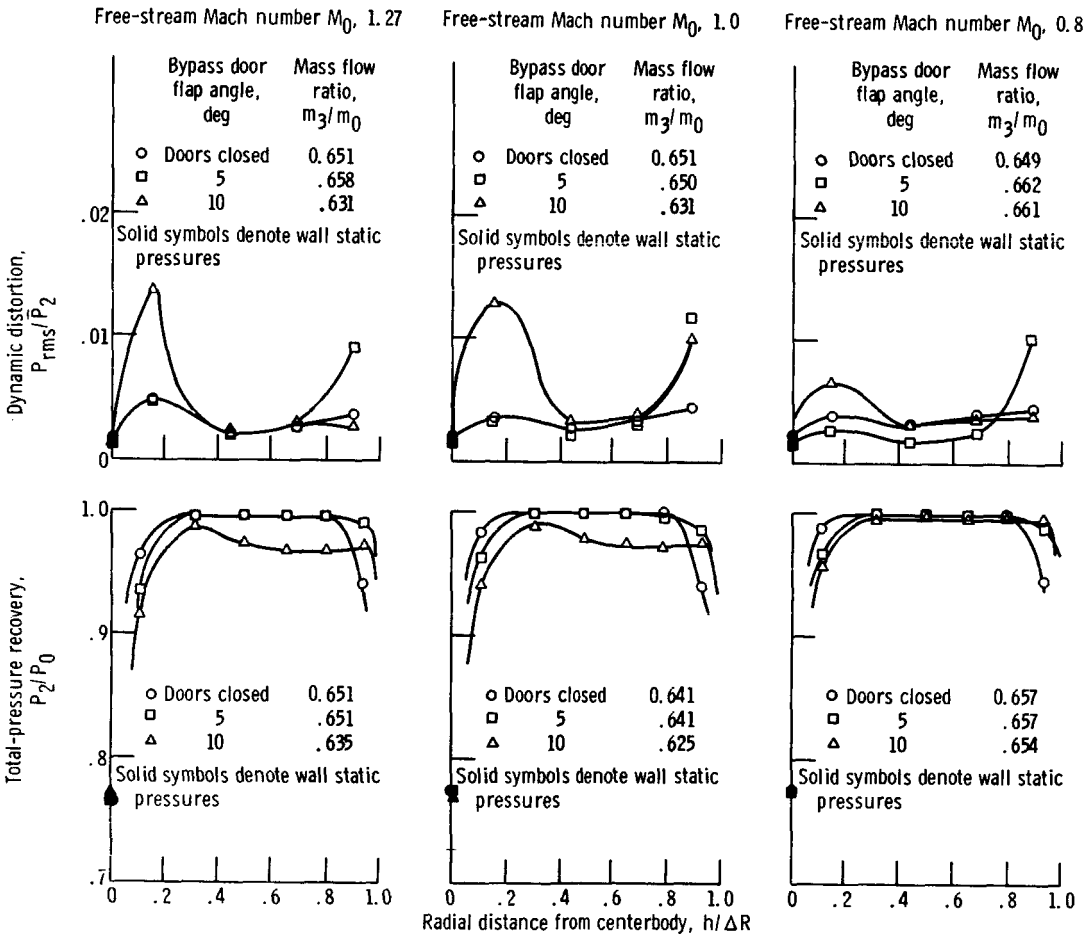

Figure 9. - Radial variation of dynamic distortion and total-pressure recovery of 60-40 inlet near design corrected weight flow.

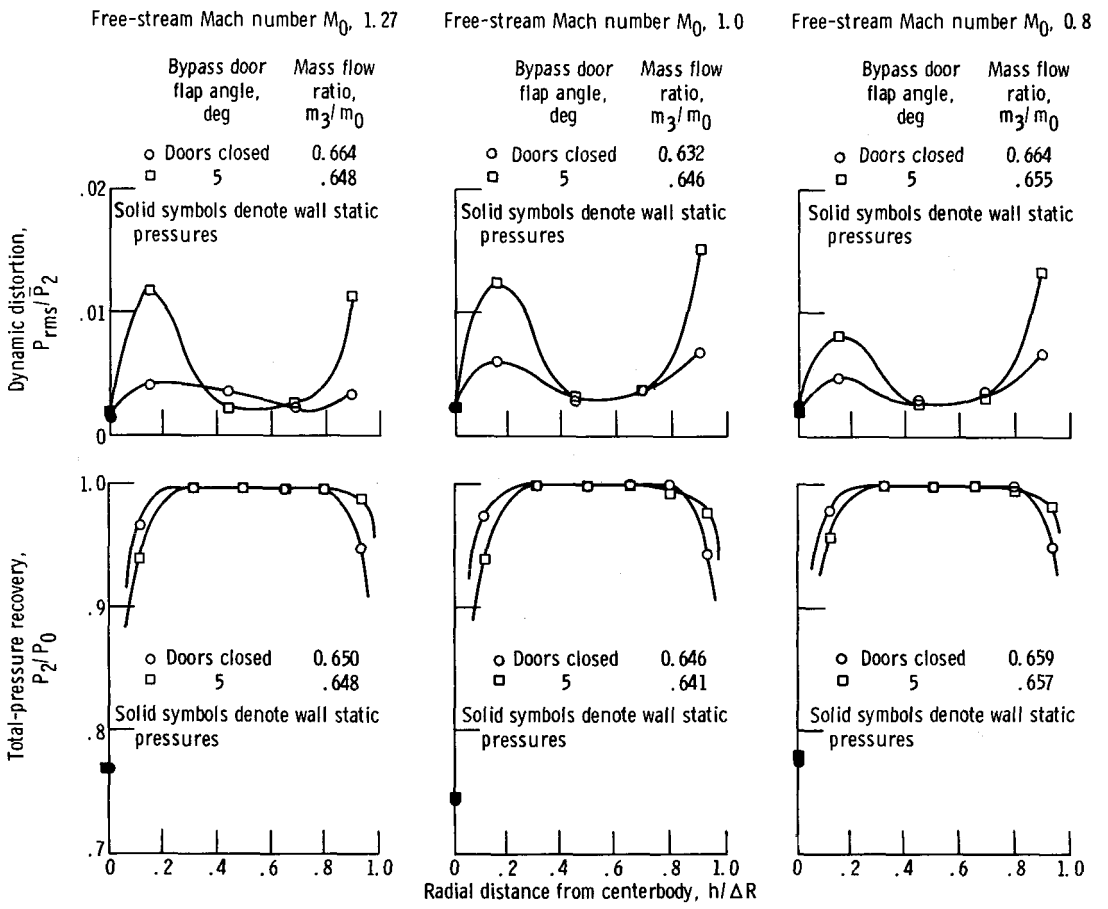

Figure 10. - Radial variation of dynamic distortion and total-pressure recovery of 40-60 inlet near design corrected weight flow.

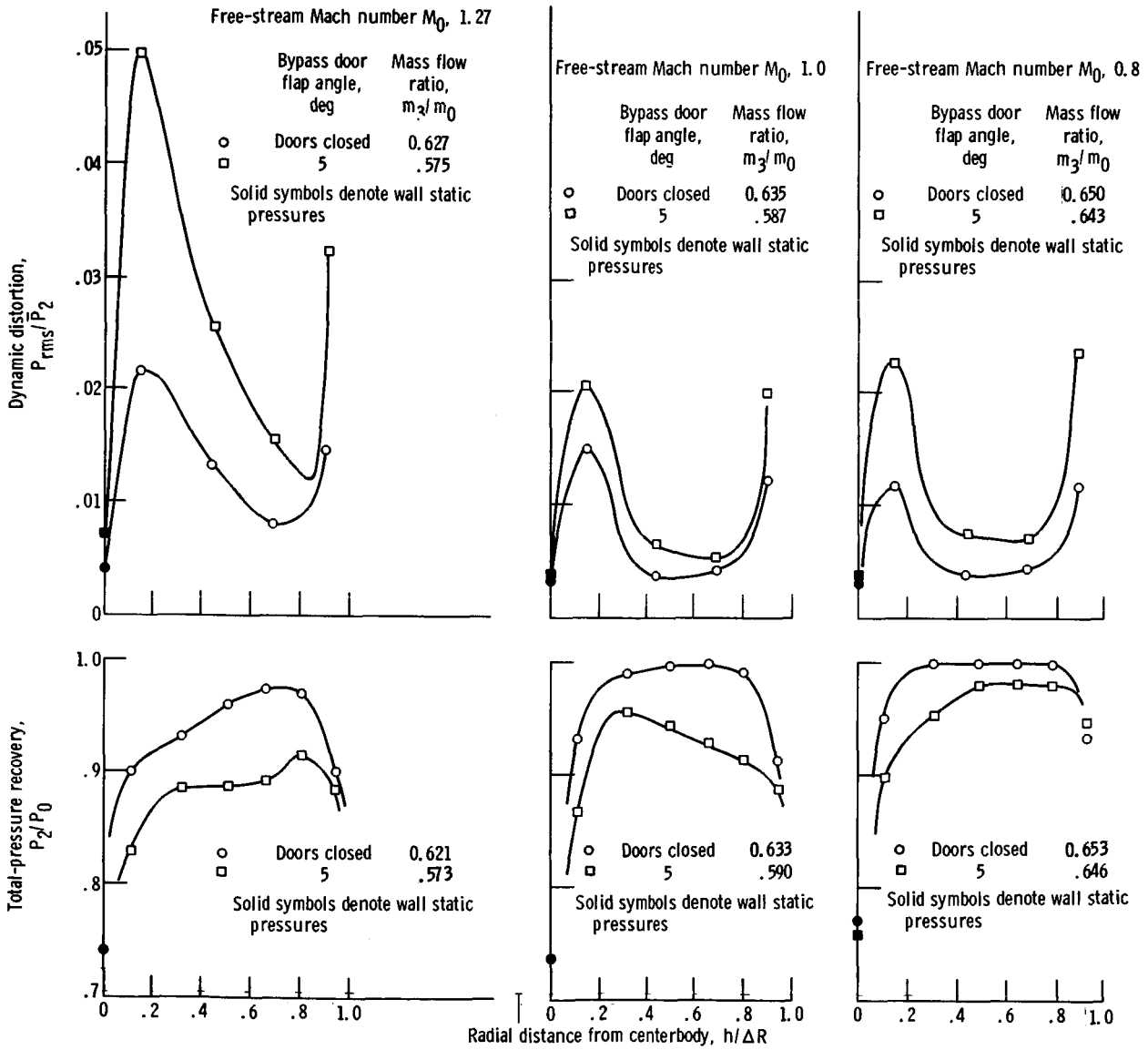

Figure 11. - Radial variation of dynamic distortion and total-pressure recovery of 30-70 inlet near design corrected weight flow.

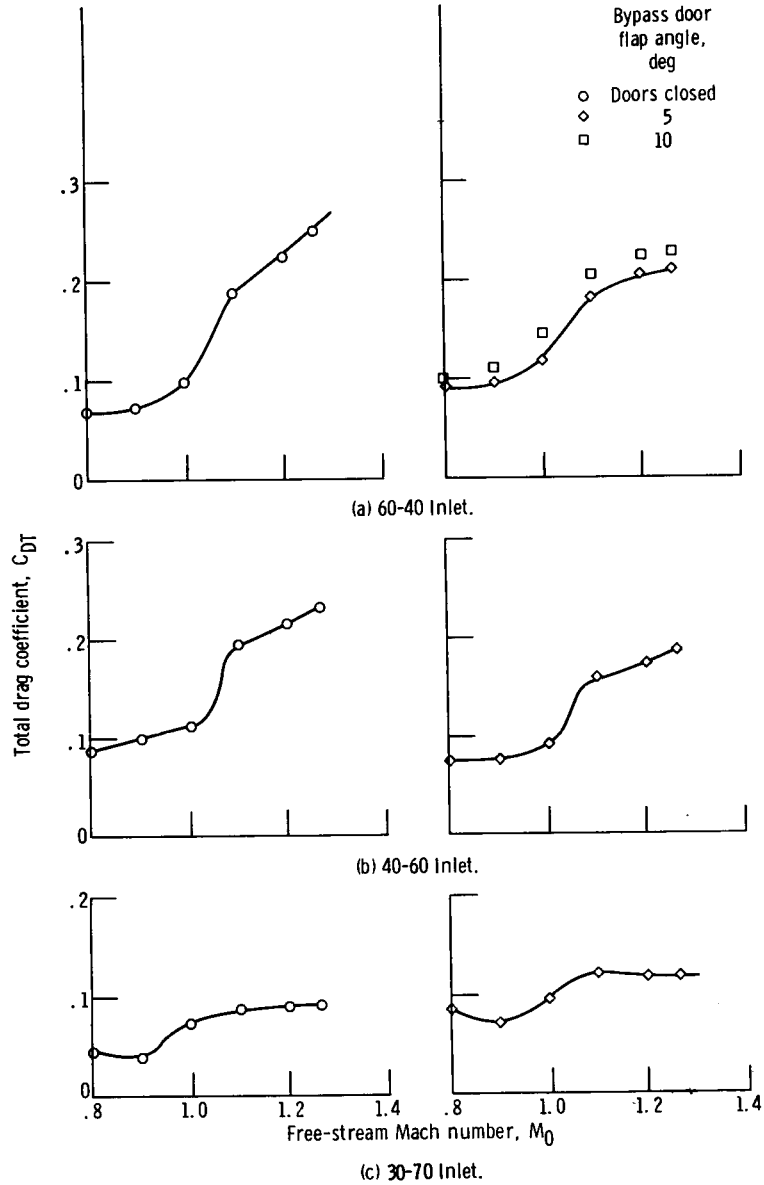

Figure 12. - Summary of drag performance of various inlets with multiple-flap bypass doors at design corrected weight flow.

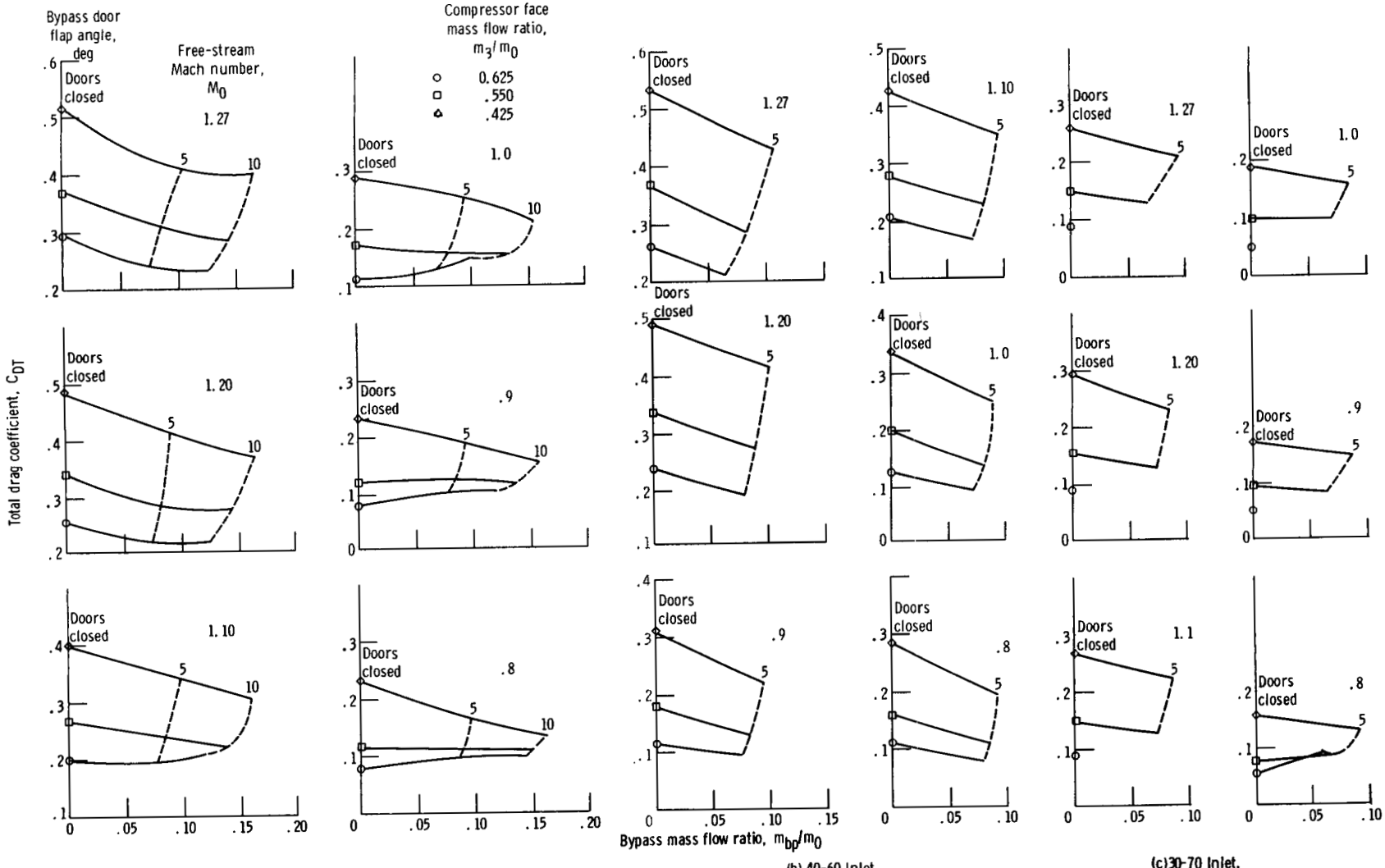

Figure 13. - Total drag coefficient of various inlets as function of bypass spillage at various compressor face mass flow ratios.

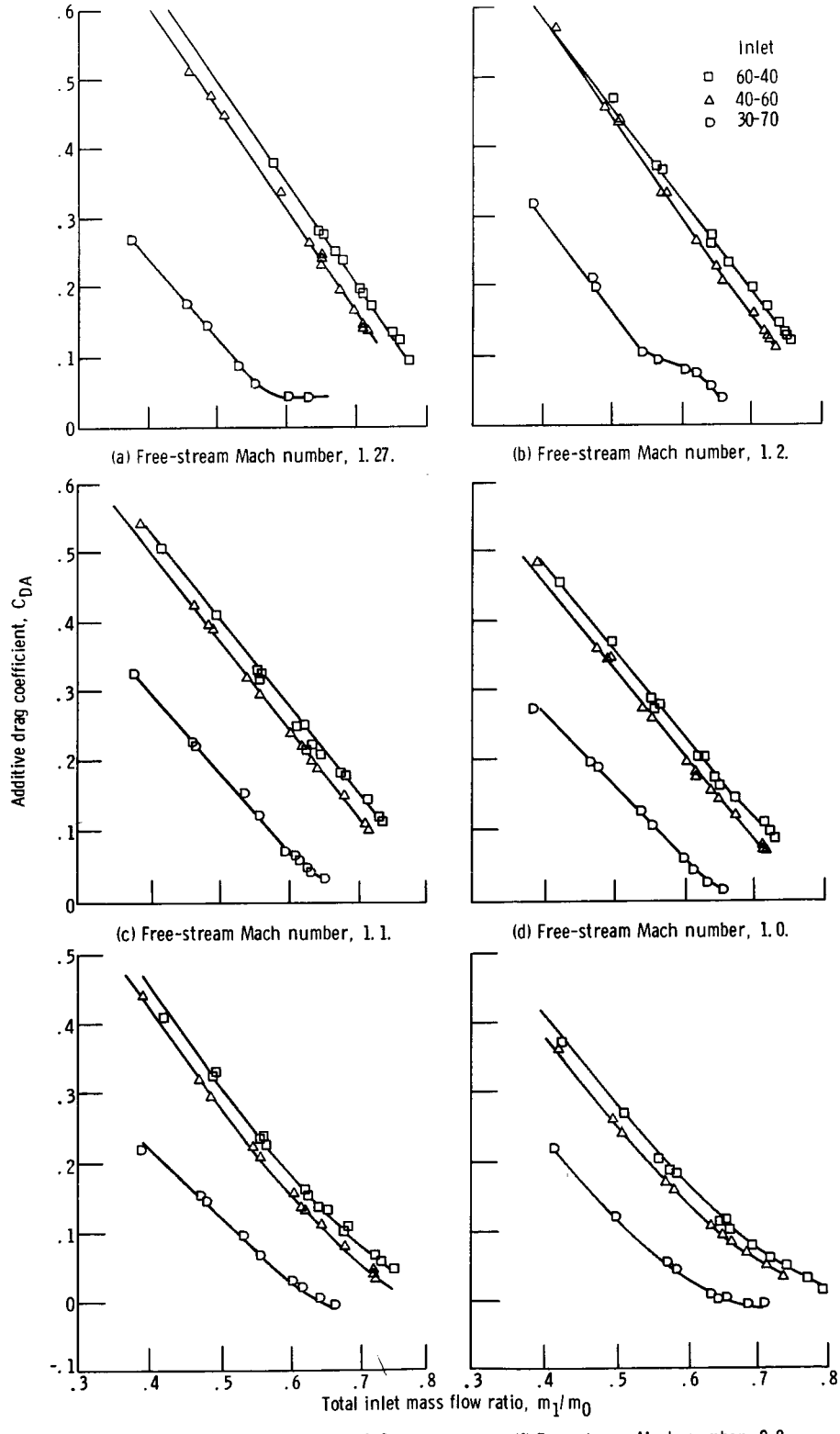

Figure 14. - Additive drag coefficient as function of total inlet mass flow ratio for various inlets.

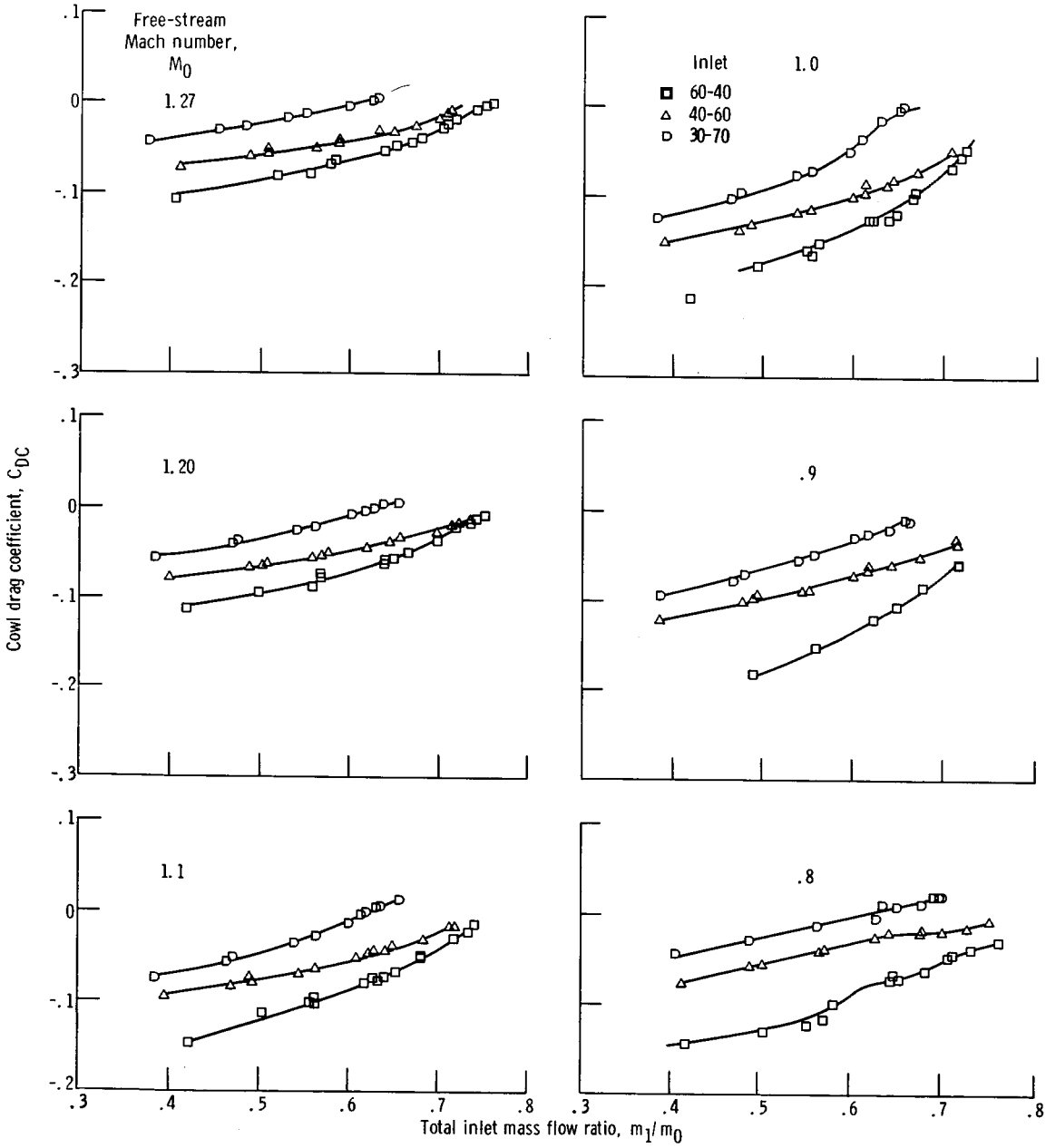

Figure 15. - Cowl drag coefficient of various inlets as function of total inlet mass flow ratio.

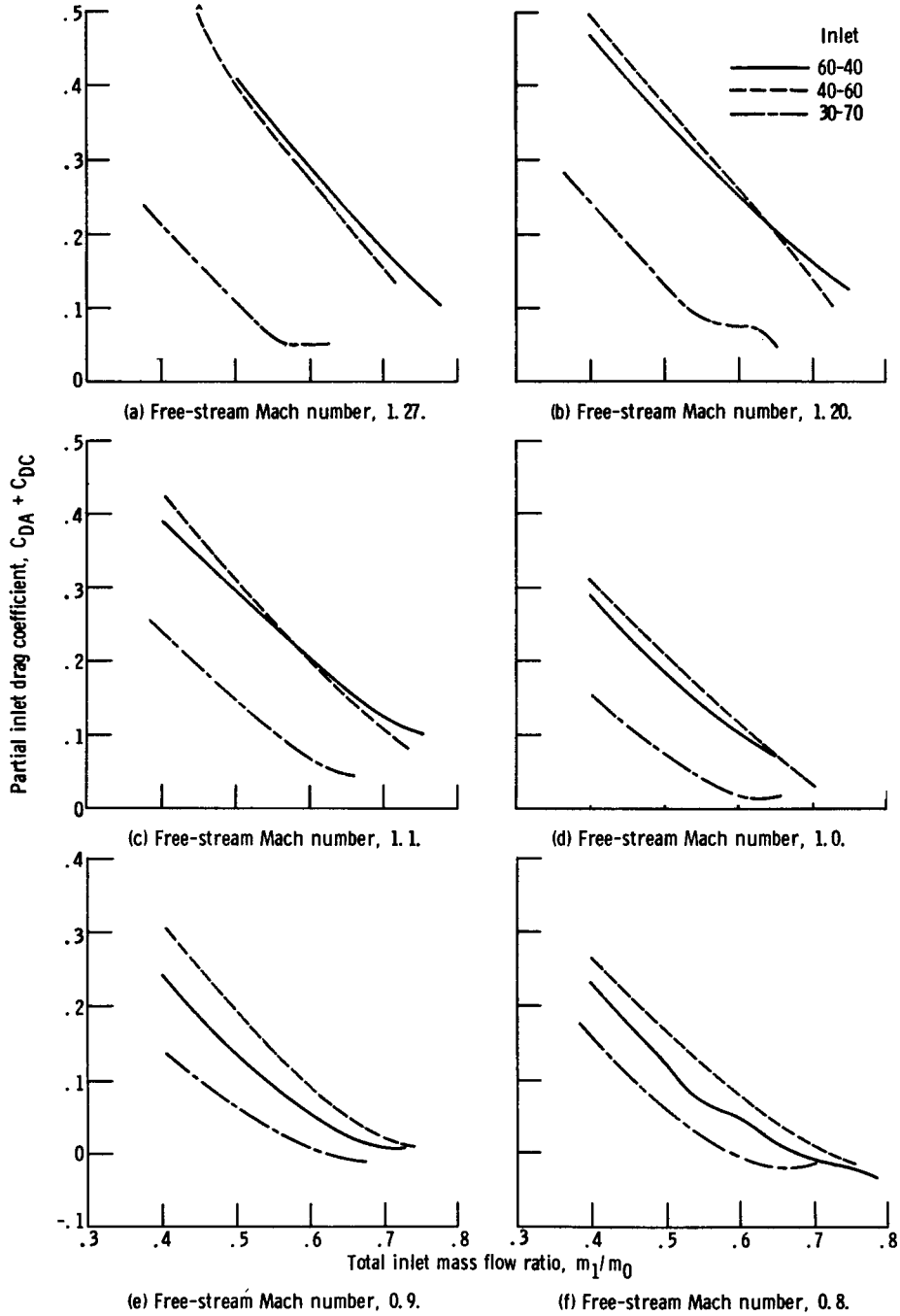

Figure 16. - Partial inlet drag coefficient of various inlets as function of total inlet mass flow ratio.

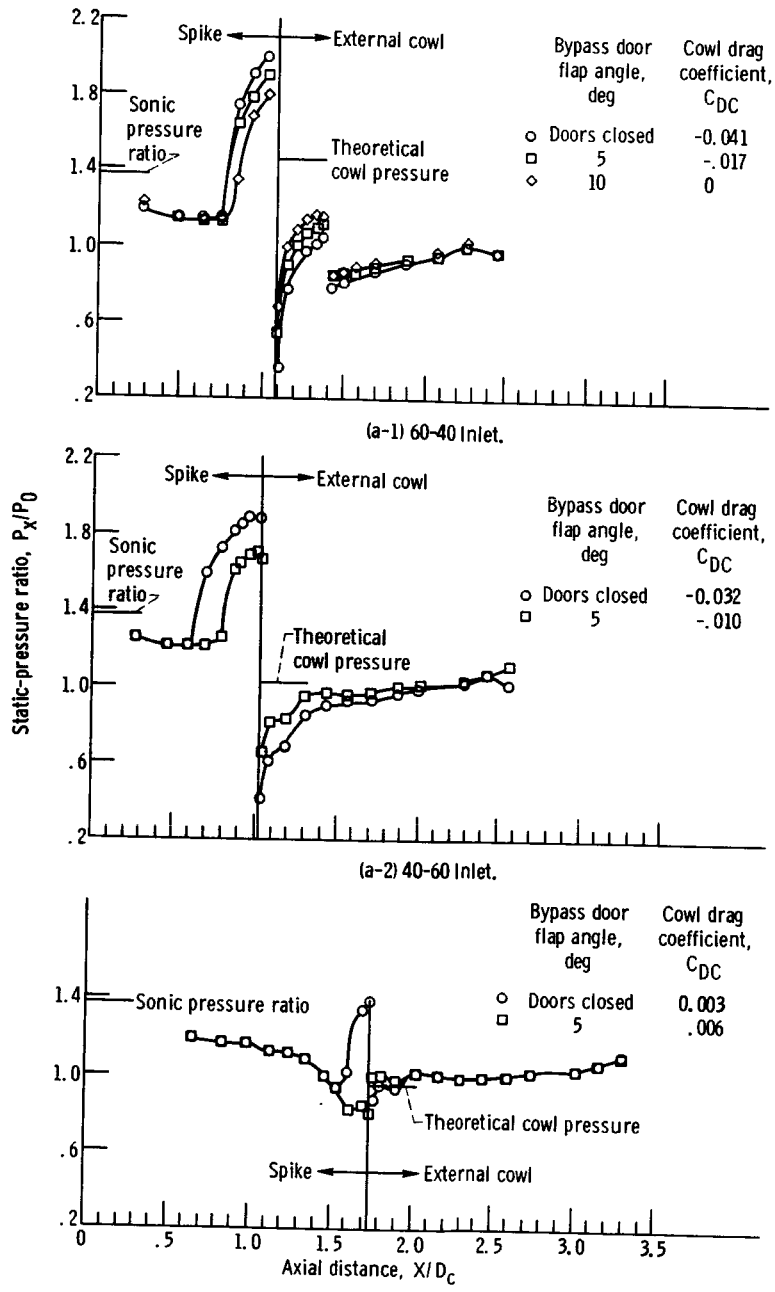

(a) Free-stream Mach number, 1.27.

Figure 17. - Static-pressure ratio along spike and cowl of various inlets at design mass flow.

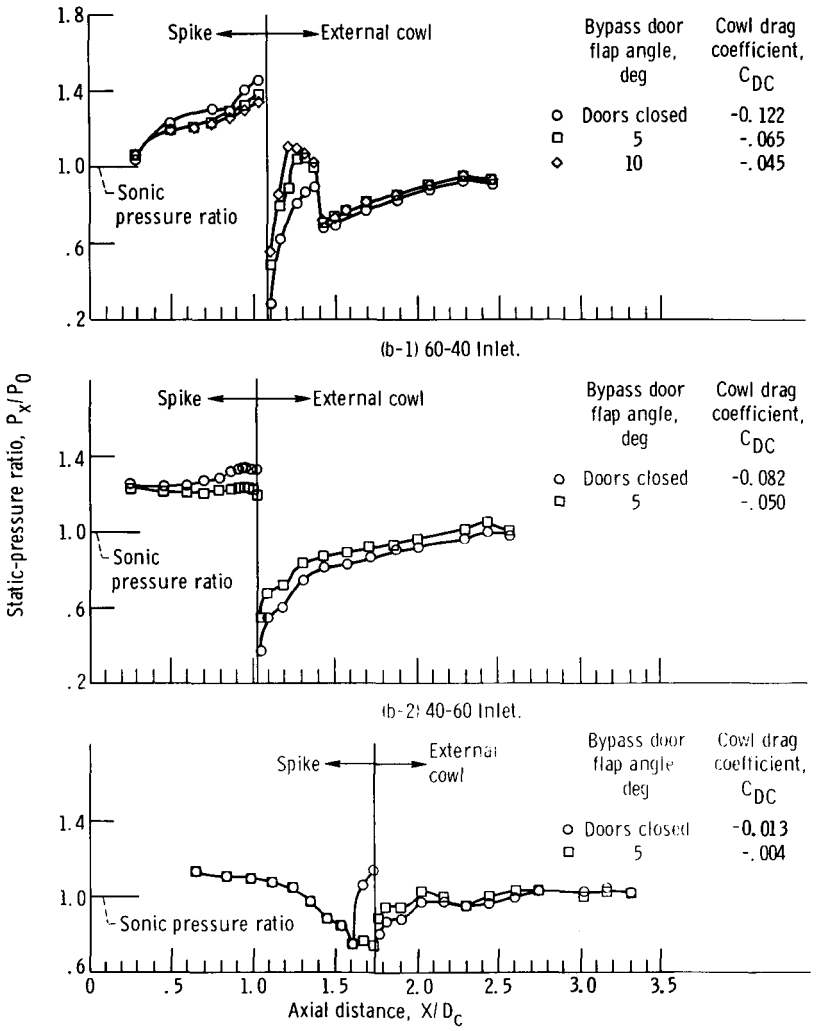

(b) Free-stream Mach number, 1.0.

Figure 17. - Continued.

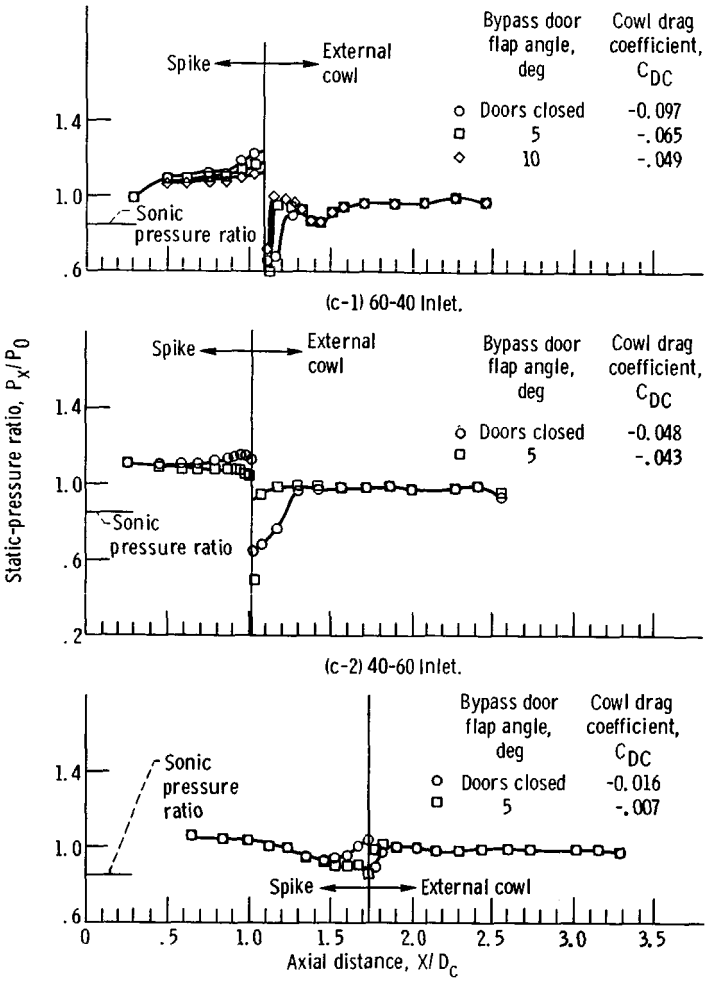

(c) Free-stream Mach number, 0.8.

Figure 17. - Concluded.

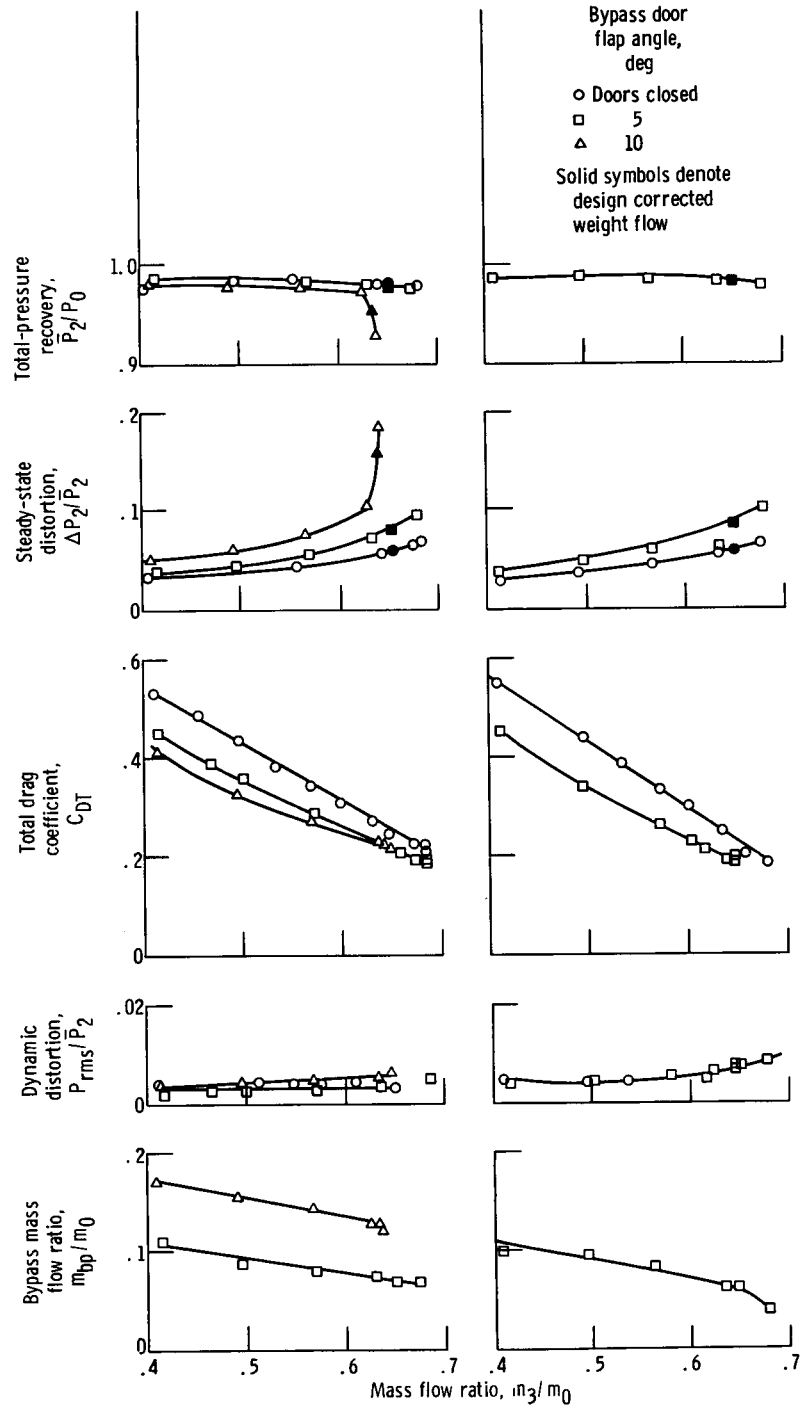

(a) 60-40 Inlet.

(b) 40-60 Inlet.

Figure 18. - General inlet performance at free-stream Mach number of 1.27.

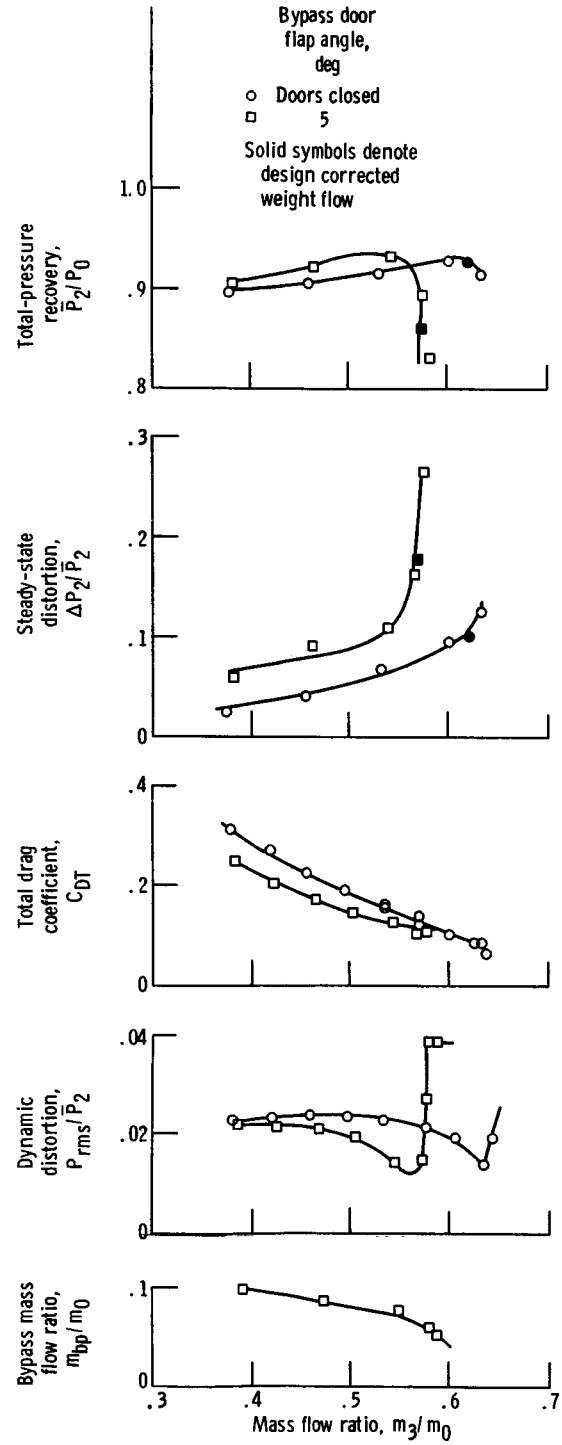

(c) 30-70 Inlet.

Figure 18. - Concluded.

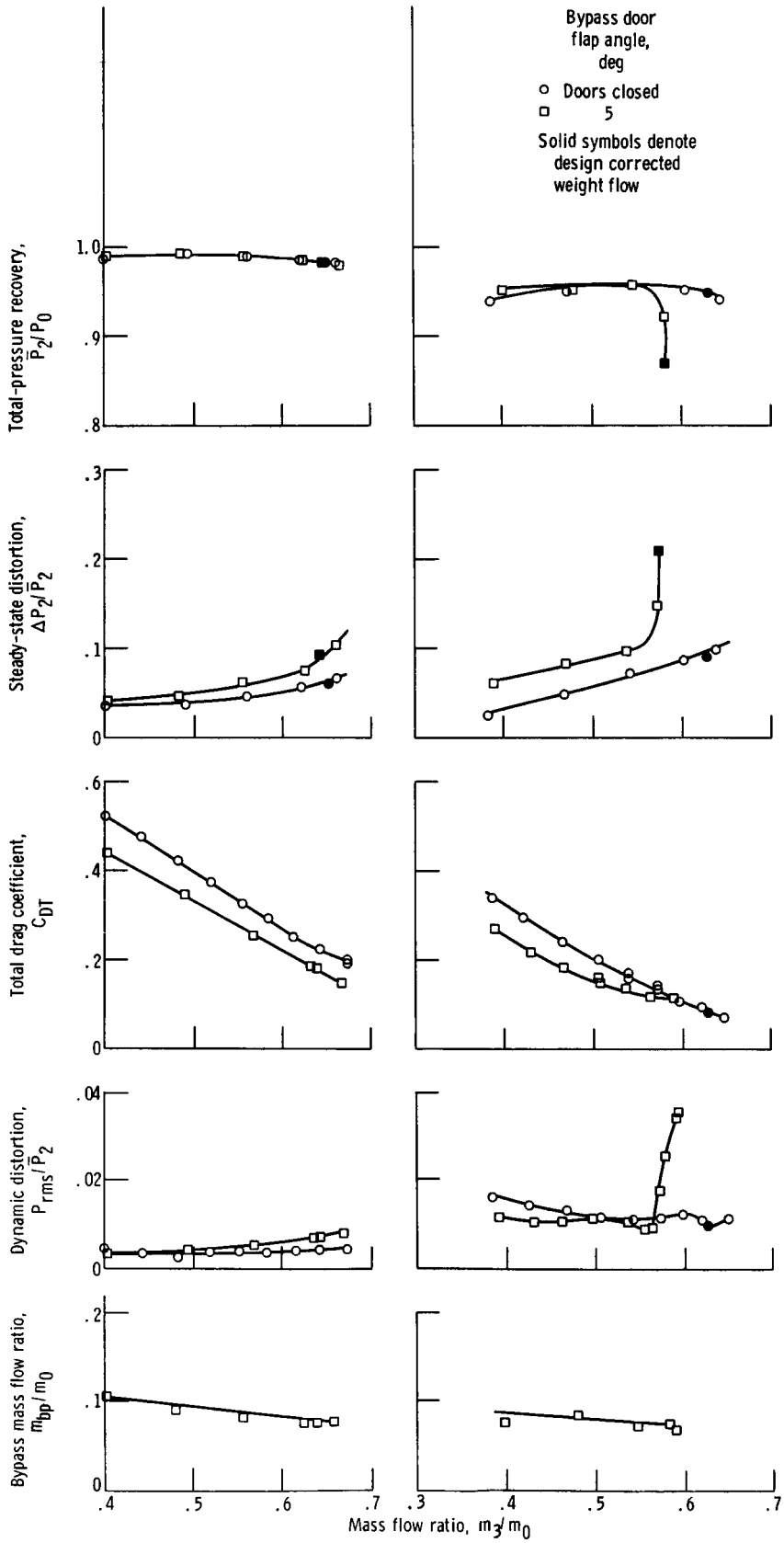

(b) 40-60 Inlet.

(c) 30-70 Inlet.

Figure 19. - Concluded.

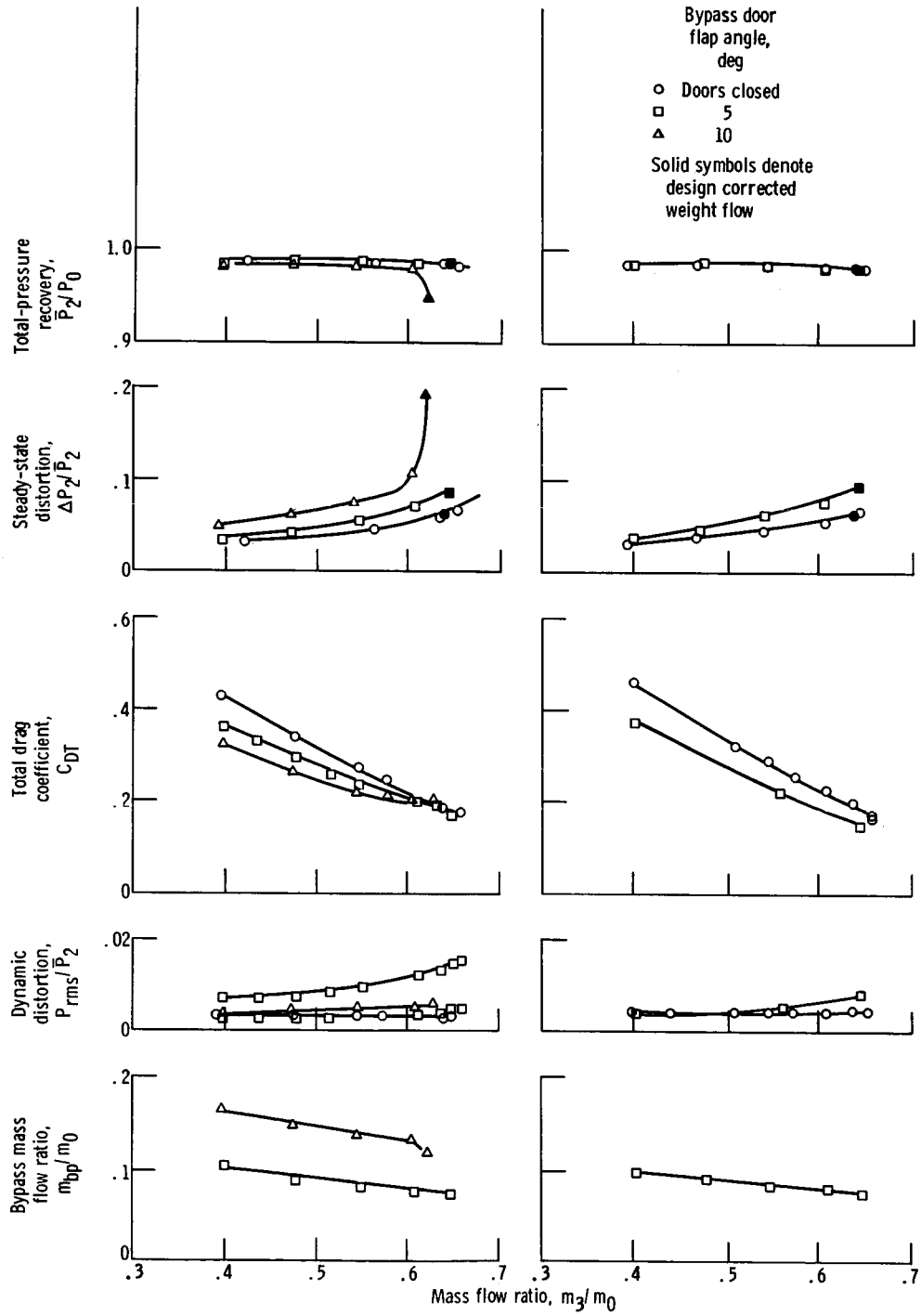

(a) 60-40 Inlet.

(b) 40-60 Inlet.

Figure 20. - General inlet performance at free-stream Mach number of 1.1.

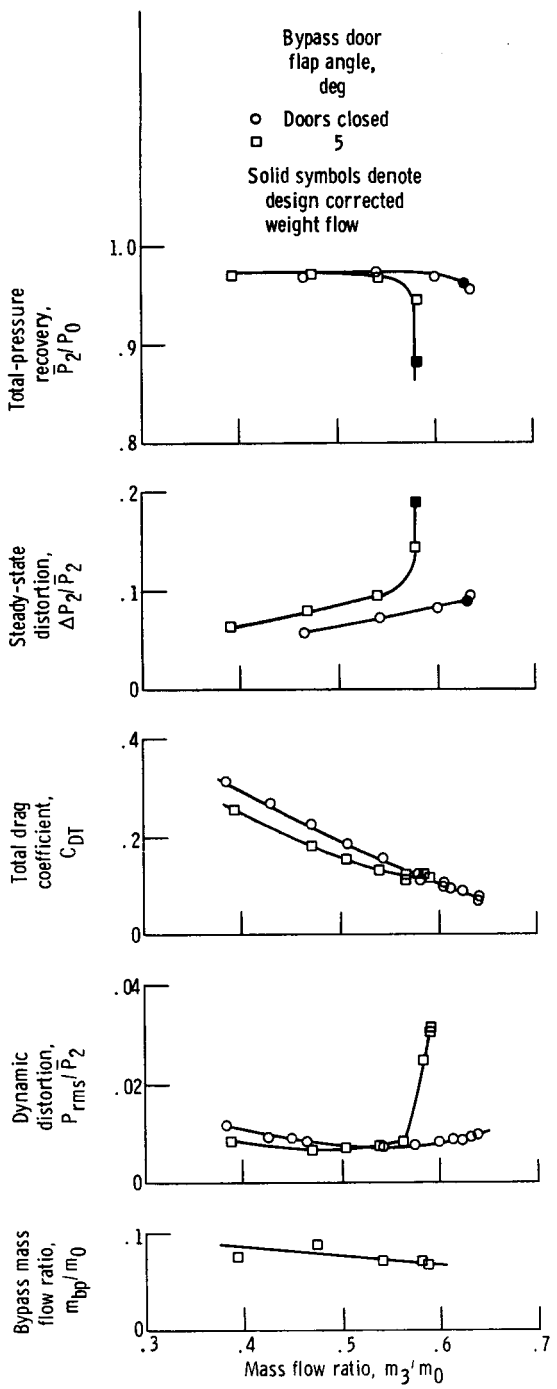

(c) 30-70 Inlet.

Figure 20. - Concluded.

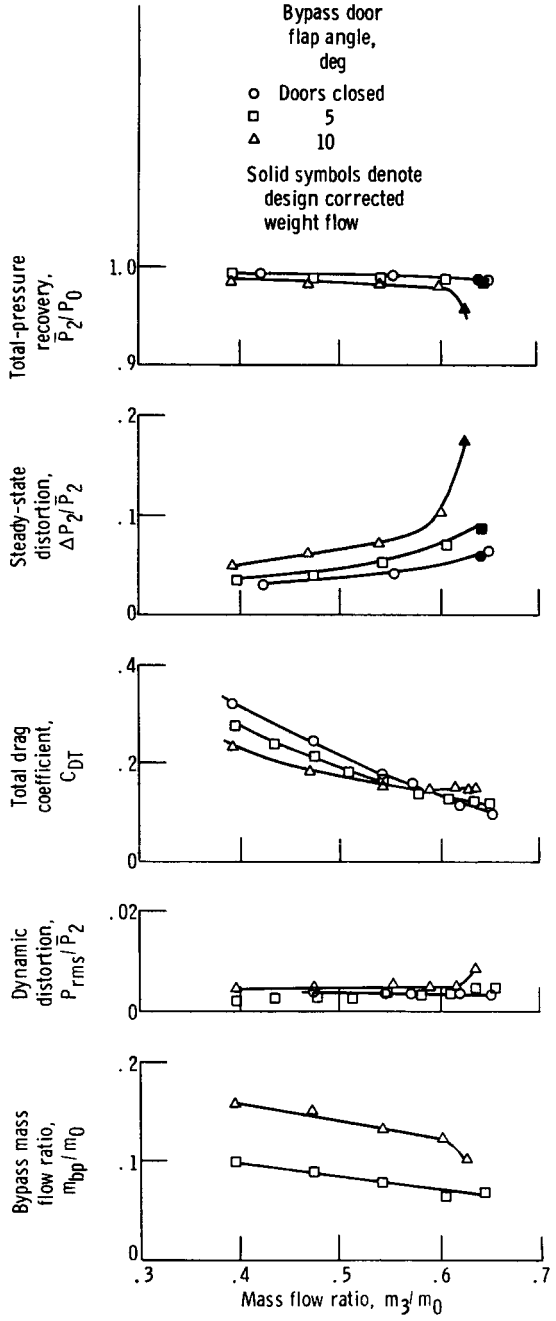

(a) 60-40 Inlet.

Figure 21. - General inlet performance at free-stream Mach number of 1.0.

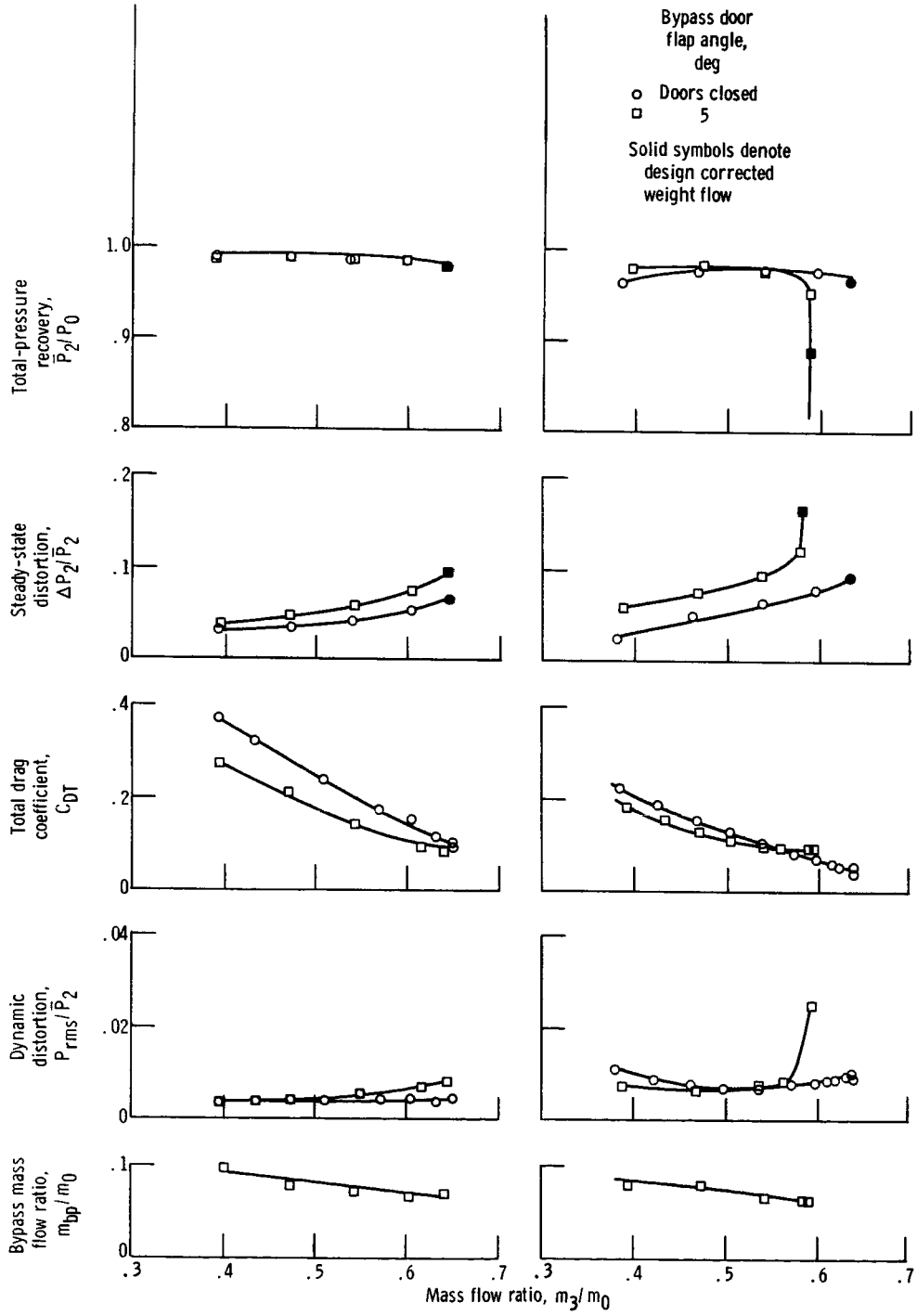

(b) 40-60 Inlet.

(c) 30-70 Inlet.

Figure 21. - Concluded.

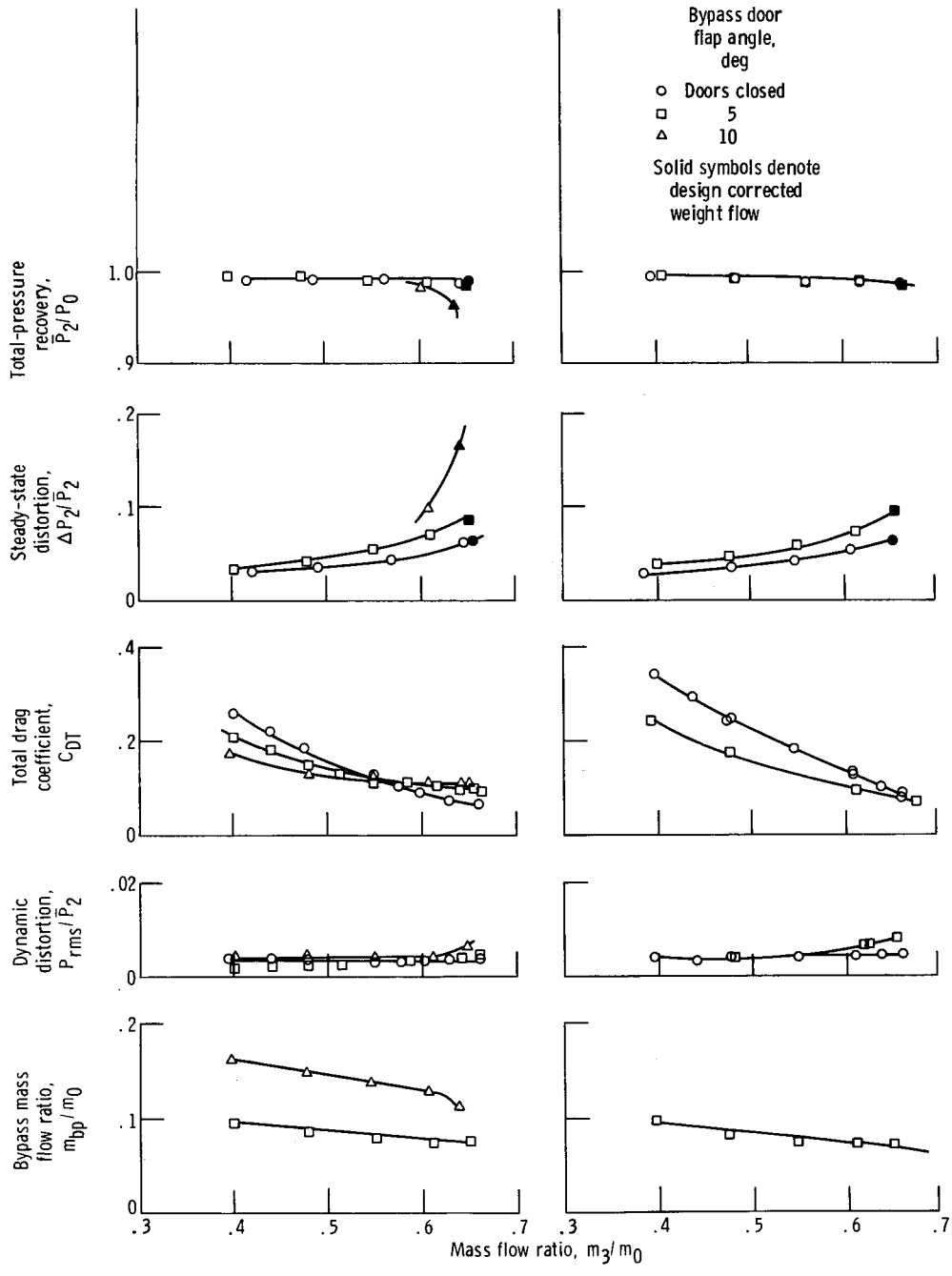

(a) 60-40 Inlet.

(b) 40-60 Inlet.

Figure 22. - General inlet performance at free-stream Mach number of 0.9.

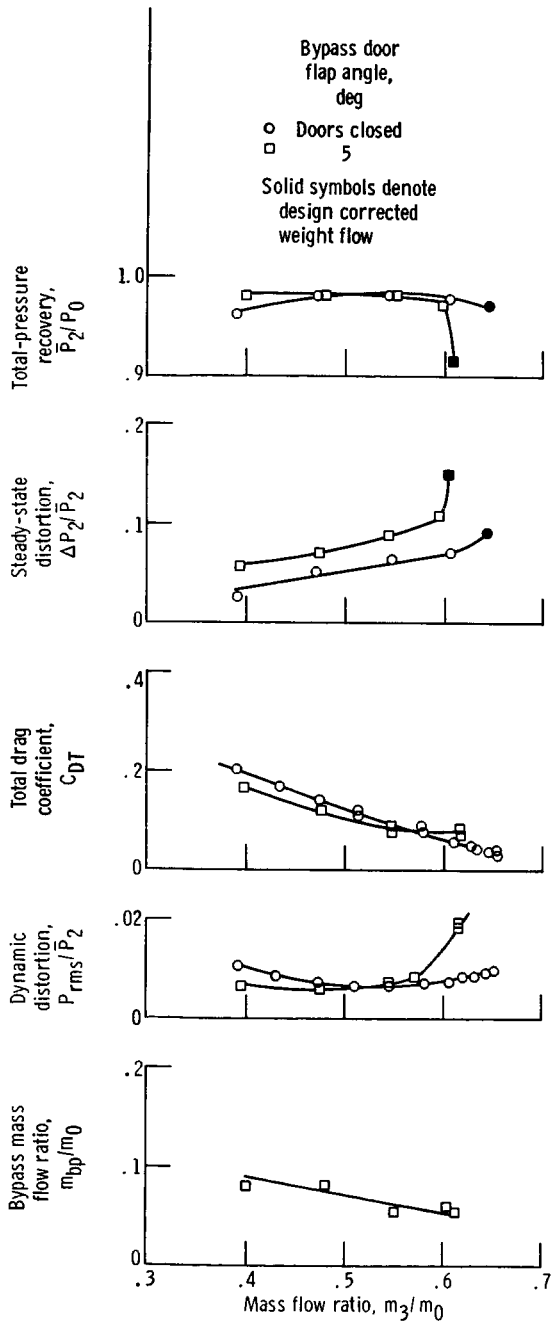

(c) 30-70 Inlet.

Figure 22. - Concluded.

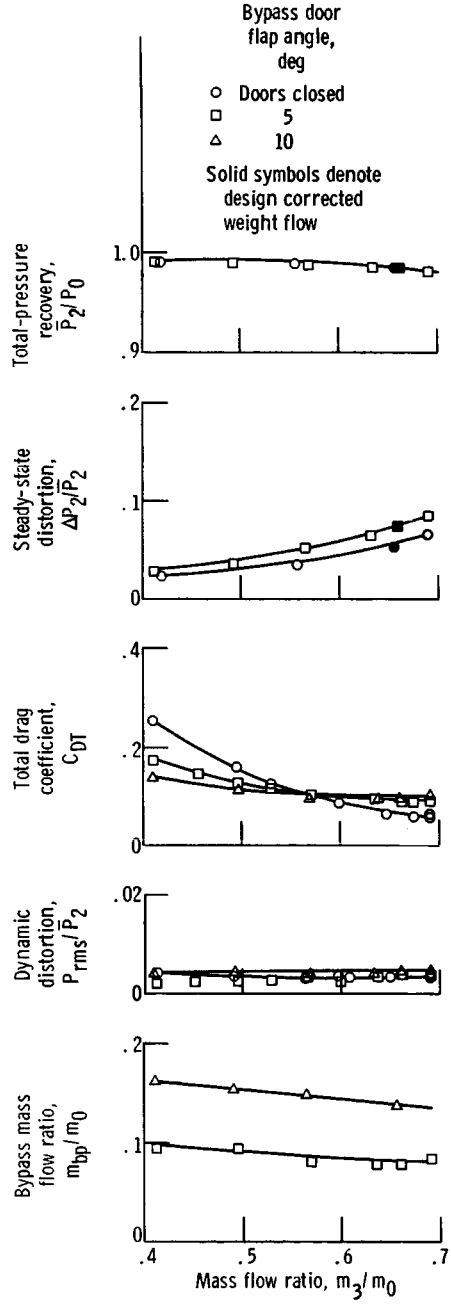

(a) 60-40 Inlet.

Figure 23. - General inlet performance at free-stream Mach number of 0.8.

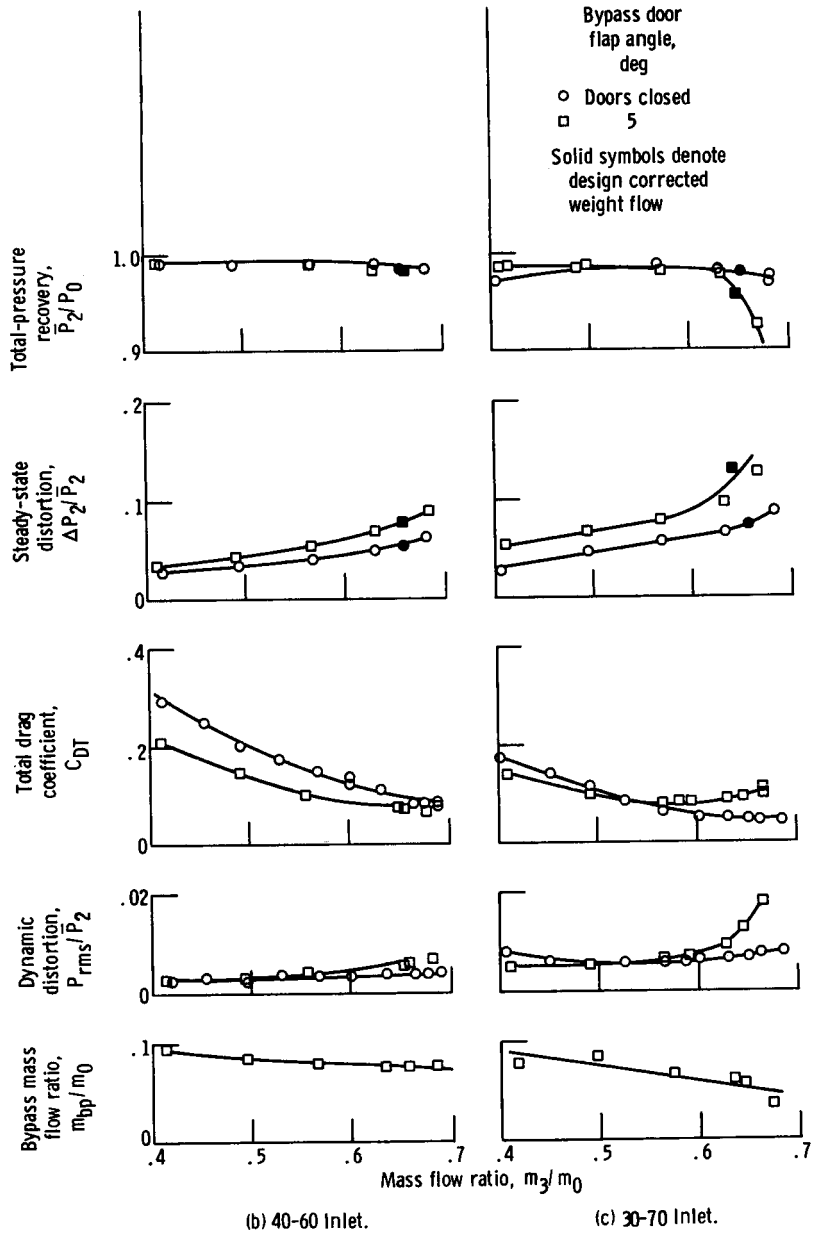

(b) 40-60 Inlet.

(c) 30-70 Inlet.

Figure 23 - Concluded.